January 2015

TRAINING AND EVALUATION OF VIRTUAL SENSORS FOR ROOFTOP UNITS

Jebaraj Vasudevan
Purdue University

Graduate School Form 30
Updated 1/15/2015

PURDUE UNIVERSITY
GRADUATE SCHOOL
Thesis/Dissertation Acceptance

This is to certify that the thesis/dissertation prepared

By JEBARAJ VASUDEVAN

Entitled

TRAINING AND EVALUATION OF VIRTUAL SENSORS FOR ROOFTOP UNITS

For the degree of MASTER OF SCIENCE IN MECHANICAL ENGINEERING

Is approved by the final examining committee:

JAMES E. BRAUN
Co-chair

TRAVIS HORTON
Co-chair

ECKHARD GROLL

To the best of my knowledge and as understood by the student in the Thesis/Dissertation Agreement, Publication Delay, and Certification Disclaimer (Graduate School Form 32), this thesis/dissertation adheres to the provisions of Purdue University's "Policy of Integrity in Research" and the use of copyright material.

Approved by Major Professor(s): JAMES E. BRAUN

Approved by: GANESH SUBBARAYAN 8/14/2015

Head of the Departmental Graduate Program Date

TRAINING AND EVALUATION OF VIRTUAL SENSORS FOR ROOFTOP UNITS

A Thesis

Submitted to the Faculty

of

Purdue University

by

Jebaraj Vasudevan

In Partial Fulfillment of the

Requirements for the Degree

of

Master of Science in Mechanical Engineering

December 2015

Purdue University

West Lafayette, Indiana

ACKNOWLEDGEMENTS

It is my pleasure to thank many people without whom this thesis may not have been possible. Foremost, I would like to express my sincere gratitude to my advisors Prof. James E. Braun and Prof. Travis Horton for their thoughtful suggestions and extended support throughout this work. I would like to especially thank Prof. James E. Braun for coping with my inexperienced writing and presentation skills and giving timely suggestions to improve them. I would also like to extend my thanks to Prof. Eckhard Groll for serving on my thesis committee and for his valuable suggestions.

Furthermore, I would like to thank Frank Lee and Bob Brown for helping me immensely to setup my experiments in a timely manner and being always there to assist me when needed. I would like to say a big thanks to my colleague Andy Hjortland for helping and guiding me throughout the course of my research. In addition to this many people have been a part of my graduate education and I am thankful to all of them.

Finally, I would like to thank Consortium for Building Energy Innovation (CBEI) and Lennox International for supporting this project.

TABLE OF CONTENTS

Page

LIST OF TABLES

Table Page

LIST OF FIGURES

Figure Page

NOMENCLATURE

Symbols

$c_{pa,cond}$	Specific heat capacity of condenser air [J/kg-K]
h	Enthalpy [J/kg]
$h_{in,ref,evap}$	Evaporator inlet refrigerant enthalpy [J/kg]
$h_{out,ref,evap}$	Evaporator outlet refrigerant enthalpy [J/kg]
$h_{in,ref,cond}$	Condenser inlet refrigerant enthalpy [J/kg]
$h_{out,ref,cond}$	Condenser outlet refrigerant enthalpy [J/kg]
k_{dsh}	Empirical coefficient for compressor discharge superheat [-]
k_{sc}	Empirical coefficient for condenser subcooling [-]
k_{sh}	Empirical coefficient for evaporator superheat [-]
k_{x}	Empirical coefficient for evaporator inlet quality [-]
$\dot{m}_{ref}$	Refrigerant mass flow rate [g/s]
$\dot{m}_{map}$	Compressor map based flow rate [g/s]
$m_{charge,actual}$	Actual amount of refrigerant charge [lb]
$m_{charge,rated}$	Amount of refrigerant charge at the rated condition [lb]
M	Information matrix [-]
N	Matrix of candidate points [-]

$P_{in,ref,comp}$	Compressor inlet pressure [kPa]
$P_{out,ref,comp}$	Compressor discharge pressure [kPa]
$P_{out,ref,cond}$	Condenser outlet pressure [kPa]
$\dot{Q}_{cooling,ref}$	Refrigerant cooling capacity [kW]
T_{sc}	Condenser outlet subcooling [C]
$T_{sc,rated}$	Condenser outlet subcooling at the rated condition [C]
T_{sh}	Evaporator outlet superheat [C]
$T_{sh,rated}$	Evaporator outlet superheat at the rated condition [C]
T_{dsh}	Compressor discharge superheat [C]
$T_{dsh,rated}$	Compressor discharge superheat at the rated condition [C]
$T_{out,ref,evap}$	Evaporator refrigerant outlet temperature [C]
$T_{out,ref,cond}$	Condenser refrigerant outlet temperature [C]
$T_{sat,evap}$	Saturation temperature of the evaporator [C]
$T_{sat,cond}$	Saturation temperature of the condenser [C]
$T_{out,ref,comp}$	Compressor discharge temperature [C]
$T_{out,air,cond}$	Condenser air outlet temperature [C]
$T_{in,air,cond}$	Condenser air inlet temperature [C]
$\dot{W}_{comp}$	Compressor input power [W]
X	Design matrix of candidate points [-]

ρ_{xy}	Pearson product-moment correlation [-]
ρ_{new}	Suction density at operating condition [kg/m^3]
ρ_{map}	Suction density at map-based condition [kg/m^3]
σ_T	Individual thermocouple uncertainty [C]
$\sigma_{T,ave}$	Average thermocouple uncertainty [C]
ω_A	Uncertainty in the calculated variable
ω_{zi}	Uncertainty in the measured variable
$\Delta(x_i, x^j)$	Fedorov Delta function

Abbreviations

AHRI	Air-conditioning, Heating and Refrigeration Institute
ASME	American Society of Mechanical Engineers
COP	Coefficient of Performance
ECM	Electronically Commutated Motors
FDD	Fault Detection and Diagnostics
HVAC	Heating, Ventilation and Air-conditioning
LAN	Local Area Network
OEM	Original Equipment Manufacturer
PWM	Pulse Width Modulation
RMSE	Root Mean Square Error
RTU	Rooftop unit
SEER	Seasonal Energy Efficiency Ratio

TXV	Thermal Expansion Valve
VFD	Variable Frequency Drive
VRC	Virtual Refrigerant Charge
VCP	Virtual Compressor Power

ABSTRACT

Vasudevan, Jebaraj. M.S.M.E., Purdue University, December 2015. Training and Evaluation of Virtual Sensors for Rooftop Units. Major Professors: James E. Braun and Travis Horton, School of Mechanical Engineering.

This thesis focuses on assessing and extending specific virtual sensors for rooftop units with micro-channel condensers, which are a growing part of the market. The rooftop unit virtual sensors provide low-cost measurements of the amount of refrigerant charge, cooling capacity and compressor power and are expected to be embedded within manufactured products in the factory. In addition, a low-cost approach for training the virtual refrigerant charge sensor in an open lab space was proposed and evaluated. The accuracy of virtual rooftop unit sensors were evaluated over a wide range of conditions using measurements obtained in environmental (psychrometric) chambers and were generally within ±10% of the values determined from more direct measurements. The concept of low-cost open lab training for virtual charge sensor along with some guidelines to choose open lab training points was evaluated and found to give similar accuracy as sensors trained using a wide range of operating conditions. The total cost of embedding the three virtual sensors in a rooftop unit at a factory would be in the range of $60 to $120 per unit. This is much less than the cost of directly measuring only two of the three quantities: unit cooling capacity and compressor power. There is no practical direct measurement method for the amount of refrigerant charge to enable cost comparisons with the cost of virtual charge sensing.

CHAPTER 1. INTRODUCTION

1.1 Background and Motivation

In order to improve existing fault detection and diagnostics methodologies for heating, ventilation, and air-conditioning (HVAC) equipment, virtual sensor technology has been applied to systems to provide more useful diagnostic inputs and reduce initial sensor costs [1, 2, 3]. Virtual sensors are designed to measure quantities that are normally expensive or impossible to measure directly using other lower cost measurements and mathematical models relating these measurements to the desired quantity.

Previous work on virtual sensors for vapor compression cooling and heating equipment has focused on the development and evaluation of sensors for different types of equipment, including RTUs, split-type residential heat pumps, and variable refrigerant flow multi-split heat pumps [2, 4]. The equipment has included different types of components, including single-speed and variable-speed compressors and different types of expansion valves, including short-tube fixed orifices, thermostatic expansion valves, and electronic expansion valves. However, none of the previous work has considered equipment having a micro-channel condenser or evaporator. RTUs with micro-channel condensers are gaining market share and the use of micro-channel evaporators is likely to occur in the near term. Micro-channel heat exchangers have much less internal volume per unit surface and therefore contain much lower mass of refrigerant during operation.

The reduction in charge for units with micro-channel condensers can be on the order of 50% compared with similarly sized units with conventional fin-tube condensers. As a result, the sensitivity of RTU performance to the mass of refrigerant charge is greater than for units that employ conventional fin-tube heat exchangers and there is a need to evaluate the accuracy of virtual charge sensors for this type of equipment.

One other motivation for improved FDD tools is the regulatory requirements of future HVAC equipment. In response to the 2013 California Title 24 requirements, RTU manufacturers are required to provide integrated tools capable of detecting and diagnosing problems associated with outdoor air economizers (OAE) [5]. The next revision of California Title 24 requirements may include more RTU diagnostics requirements such as improper refrigerant charge levels or condenser and evaporator fouling [6]. Past studies have shown that approximately 50% of RTUs in the U.S. may be improperly charged [7, 8, 9]. This is important because improper charge levels result in reduced cooling capacity and cooling efficiency, leading directly to increased energy usage and operating costs.

1.2 Virtual Sensors Based FDD

Virtual sensors use low-cost measurements and simple mathematical models to estimate quantities that would be expensive and/or difficult to measure directly. The use of virtual sensors can reduce costs significantly compared to the use of direct measurements. FDD is an acronym for fault detection and diagnosis. Fault detection works by comparing the expected and actual states of the system and identifies a fault in the system when the actual state of the system deviates from the expected/normal state. This provides earlier awareness of faults present in a system. Fault diagnosis works by isolating the fault from other faults present in a system and thereby provides an understanding of the nature and cause of the

fault in the system. In addition, diagnosis reduces costs for service since a service technician can more quickly determine and identify the root cause of the fault and perform corrective action to fix it.

Virtual sensor based FDD uses low-cost virtual sensors to detect and diagnose the faults present in a system. If the virtual sensors are chosen to be uniquely dependent on individual faults (e.g., air flow for fouling, refrigerant charge, etc.) then they naturally isolate individual faults from other types for diagnosis. This is a significant advantage over other residual-based diagnostics tools that often cannot handle simultaneous fault conditions. In addition, virtual sensors can be employed to provide continuous monitoring of cooling capacity, power consumption, and efficiency, which would be cost prohibitive using direct measurements. These higher-level measurements are useful for evaluating the impacts of faults within an FDD system.

1.3 Research Objectives and Approach

This project is focused on extending and assessing specific virtual sensors for rooftop unit (RTU) air conditioners. The primary objective was to extend virtual refrigerant charge, capacity, and power sensors to RTUs having micro-channel condensers. This type of equipment is a growing part of the market and its performance is more sensitive to refrigerant charge because a micro-channel condenser has significantly lower internal volume for the same heat transfer area compared to conventional fin-tube condensers.

One of our primary goals in assessing these virtual sensors was to demonstrate accuracy within 10% and the cost savings potential of virtual sensor implementation as compared to direct measurements.

One of the key technical issues in applying virtual sensors is the “calibration” or “training” necessary for the virtual sensor to provide accurate estimates of a particular quantity. For virtual sensors embedded in RTU products, the process of training/calibration needs only be done for one unit of a particular model type and can then be implemented within the manufactured products for that model. However, it is expensive and time consuming to employ environmental test (psychrometric) chambers to generate the data necessary to train virtual sensors for each model of a manufacturer’s line of RTUs. Therefore, another objective of this project was to minimize the training requirements for applying the virtual charge sensor to specific RTU model using open laboratory environment tests performed over a short period of time. The virtual sensor accuracy and training were assessed in this project using laboratory measurements for an RTU employing a micro-channel condenser.

1.4 Thesis Formulation

This chapter presented an overview of previous work in the area of virtual sensors along with the motivation behind and the approach taken to provide the contributions of this thesis.

Chapter 2 provides a description of the experimental set-up, instrumentation and testing procedures used to develop and validate the virtual sensor models in this thesis.

Chapter 3 describes the various virtual sensor model forms for measuring refrigerant charge, compressor power and cooling capacity. Furthermore, these models are validated in this chapter. Also, the cost savings potential of virtual sensor implementation over direct measurements is presented.

A methodology to minimize the training requirements of the virtual charge sensor is presented in Chapter 4. The validation of this training methodology is also presented.

Finally, Chapter 5 summarizes the important results of the work reported in this thesis and gives recommendations for future work.

CHAPTER 2. EXPERIMENTATION AND DATA COLLECTION

2.1 Experimental Goals

Experiments were conducted in order to train the virtual charge sensor models and evaluate the accuracy of the charge, capacity, and power virtual sensors over a wide range of operating conditions. To support the goal of minimizing the training requirements for the virtual charge sensor models, data was collected with the rooftop unit running in an open lab environment space (see Chapter 4). Additional data was collected over a wide range of conditions with the rooftop unit operating in the psychrometric chambers and this data was used to evaluate the accuracy of all three virtual sensor models (see Chapter 3).

2.2 RTU Selection and Description

A Lennox 5-ton packaged high-efficiency rooftop unit with a SEER rating of 17.0 was used to perform the experiments. This rooftop unit has an all-aluminum micro-channel condenser coil with much smaller volume compared to a conventional round tube plate fin condenser and has only a nominal R410A refrigerant charge of 7.05 lbs. It also features a dual stage scroll compressor to respond efficiently to varying loads with operation in second stage for higher loads (e.g., on hot summer days) and first stage for milder loads. Furthermore, it has a thermal expansion valve (TXV) and a round tube plate fin evaporator. The indoor blower and outdoor fan are driven by

variable-speed ECM direct drive motors for energy efficient multi-stage air volume operation. The rooftop unit is as shown in the Figure 1.

Figure 1. RTU used for experimentation.

2.3 RTU Instrumentation and Data Acquisition

Figure 2 presents a schematic of the refrigerant cycle that depicts the refrigerant measurement points. Table 1 defines whether each of these sensor measurements is used as an input to or validation for the virtual sensor models. The following subsections provide some description of the types of sensors used and their uncertainties.

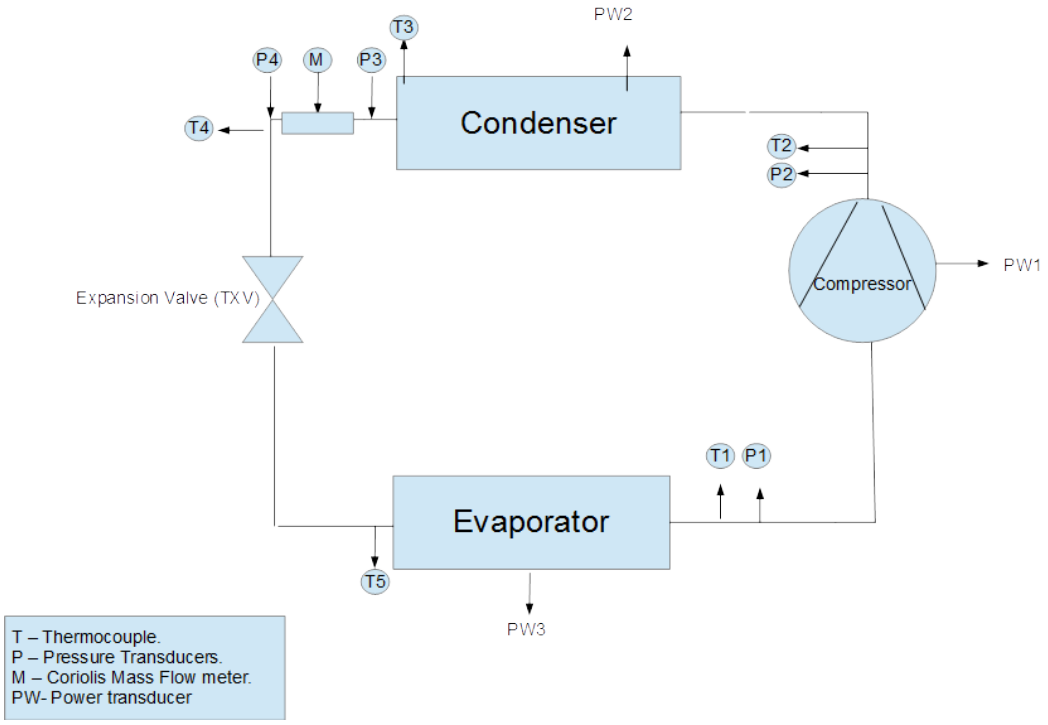

Figure 2. Refrigerant side instrumentation of the RTU.

Table 1. Refrigerant sensors used and their application.

No.	Sensors	Location of sensors	Use of sensors
1	T1-Thermocouple	Evap. outlet temp.	Virtual charge and capacity sensors
2	T2-Thermocouple	Compressor discharge temp.	Virtual charge sensor
3	T3-Thermocouple	Cond. outlet temp.	Virtual charge and capacity sensors
4	T4-Thermocouple	Mass flow meter outlet temp.	Temperature drop in the mass flow meter
5	T5-Thermocouple	Evap. inlet temp.	Virtual charge sensor

Table 1. Continued.

6	P1- Pressure transducer	Evap. suction pressure	Virtual capacity and power sensors
7	P2- Pressure transducer	Compressor discharge pressure	Alternate measurement for virtual charge, power and capacity sensors
8	P3-Pressure transducer	Cond. pressure	Virtual charge, power and capacity sensors
9	P4-Pressure transducer	Mass flow meter outlet pressure	Pressure drop in the mass flow meter
10	PW1-Power transducer	Compressor input power	Used to validate compressor input power
12	M-Coriolis mass flow rate sensor	Refrig. mass flow rate	Used to validate virtual refrigerant mass flow rate sensor

2.3.1 Refrigerant-Side Temperature Measurements

Surface mounted T-type thermocouples insulated with foam tape to ensure thermal insulation were installed on the external surfaces of tubes to measure refrigerant circuit temperatures at the following locations: evaporator outlet, compressor discharge, condenser outlet, refrigerant mass flow meter outlet and evaporator inlet. The rated accuracies of these T-type thermocouples used were ±1.0 °C.

2.3.2 Refrigerant-Side Pressure Measurements

Refrigerant pressure measurements were made at the compressor suction, compressor discharge, and condenser outlet using pressure transducers from Setra (model: M207) with

rated accuracy of ±0.13%. The pressure sensors were calibrated using a Setra sensor calibration device.

2.3.3 Refrigerant Mass Flow Measurement

A mass flow meter made by Micro motion (model: DH 25) with a rated accuracy of ±0.15% was used to measure the refrigerant mass flow rate. The mass flow meter was installed between the exit of the condenser and the inlet of the expansion device. Since the refrigerant circuit had to be modified to facilitate the installation of the mass flow meter. proper care was taken to minimize the change in the refrigerant circuit length.

2.3.4 Power Measurements

The condenser fan power was measured using a power transducer made by Ametek Power Instruments (model: PCE-15) with a rated accuracy of ±4.5W (±0.25% FS). The indoor blower power was measured using a power transducer made by Ohio Semitronics (model: PC5-020C) with a rated accuracy of ±15W (±0.5% FS). Also, the compressor input power was also measured using a power transducer made by Ohio Semitronics (model: PC5-113C) with a rated accuracy of ±40W (±0.5% FS).

2.3.5 Methodology for Refrigerant Charge Adjustment

Adjustments in refrigerant charge were made by connecting the compressor suction port to a refrigerant cylinder placed on a digital scale as shown in Figure 3. Charge was added or removed by opening a metering ball valve and solenoid valve under different operating conditions. A digital scale made by Ohaus Ranger (model: r71md35-am) having a rated accuracy of 0.001 lb. was used to determine the change in refrigerant mass within the cylinder due to adding or removing refrigerant charge to or from the system. At any time,

the amount of refrigerant charge inside the system was taken as the previously known amount plus or minus the charge added or removed.

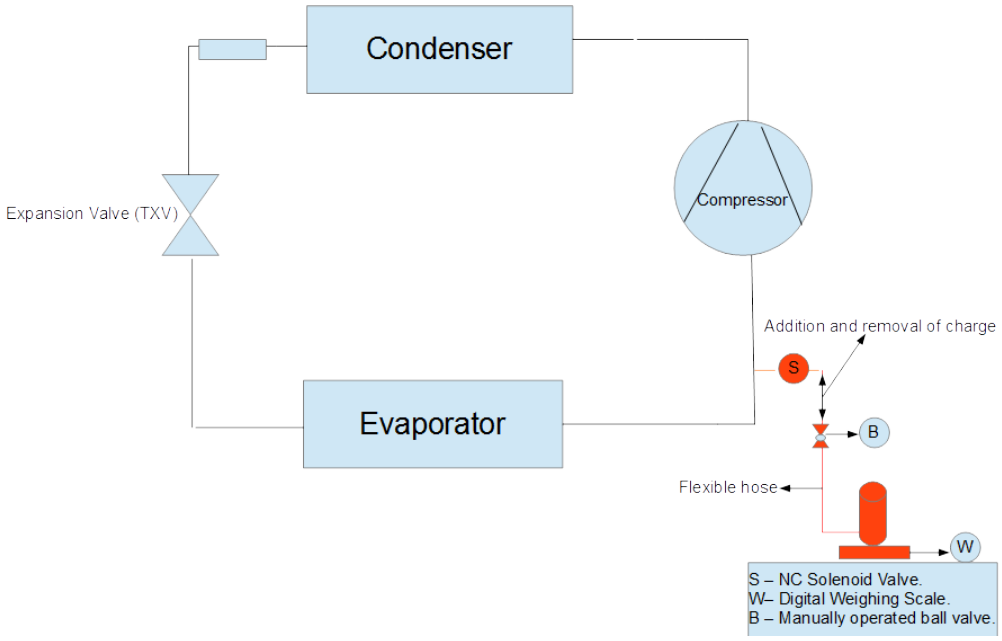

Figure 3. Methodology used for addition/removal of charge from RTU.

2.3.6 Air-Side Temperature Measurements

The temperatures of the air streams were measured using grids formed by T-type thermocouples in different locations of the rooftop unit. The return air, supply air and condenser outlet air temperatures were measured using horizontal three-by-one grids of T-type thermocouples. The air temperature at the inlet to the evaporator, which would normally be a mixed air temperature if an economizer were installed, was measured using an equally-spaced rectangular three-by-three temperature grid. Even though no economizer was installed in this study and the mixed air temperature and the air temperature in the return duct would be the nearly the same, the additional thermocouples to measure a mixed air temperature were installed to accommodate future testing with an economizer. In this

study, mixed air temperature was used because of its smaller average uncertainty (shown in Table 2) due to the use of more thermocouples in determining averages compared to the return air temperature. The condenser air inlet temperature was measured by placing five thermocouples along the entire length of the condenser diagonally and the average of these temperatures was used as the outdoor air ambient temperature to control the outdoor room temperature.

For each grid with n measurements, the average temperature T_{ave} was calculated as an arithmetic mean of the individual sensor measurements, T_i, as

$$T_{ave} = \frac{1}{n}\sum_{i=1}^{n} T_i \tag{2.1}$$

The rated accuracy σ_T of the individual T-type thermocouples was ±0.5 C. The combined uncertainty for the measurement of T_{ave} was calculated as follows,

$$\sigma_{T_{ave}} = \frac{\sigma_T}{\sqrt{n}} \tag{2.2}$$

Table 2 shows the individual and combined uncertainties of each of the thermocouple grid measurements.

Table 2. Uncertainties of the different thermocouple grids in the RTU.

Location	N	σ_T [°C]	$\sigma_{T_{ave}}$ [°C]
Return air	3	±0.5	±0.28
Supply air	3	±0.5	±0.28
Condenser air outlet	3	±0.5	±0.28
Mixed air	9	±0.5	±0.16

2.3.7 Relative Humidity and Dew Point Temperature Measurements

Relative humidity and dew point temperature measurements were measured in the return air stream before the evaporator coil and the supply air after the evaporator coil. The dew point temperature was measured using a General Eastern (model: D-2) dew point hygrometer with a two stage chilled mirror probe. It has a rated accuracy of ±0.15 °C. The relative humidity was measured using a Vaisala (model: HMD 112) humidity sensor having a rated accuracy of ±2%RH. Since the dew point hygrometers were not available during the initial phase of the testing for 30 data points, the relative humidity sensors were used to calculate the air side cooling capacity for those test data points. For all of the remaining 185 data points, dew point hygrometer measurements were used in place of relative humidity sensor measurements to calculate the air side cooling capacity. Since the relative humidity sensors were less accurate than the dew point hygrometers, they result in higher cooling capacity uncertainties as shown in Table 4.

2.3.8 Air Flow Measurements

An ASME standard nozzle box was used to measure the supply air flow rate of the rooftop unit. The nozzle combinations of 4” and 6” nozzles were chosen such that the acceptable measurement range closely matched the target air flow rate. An Endress and Hauser (model Deltabar M PMD55) differential pressure transmitter with a rated accuracy of ±0.1% was used to measure the nozzle pressure drop. In order to calculate the density of the supply air at the nozzle inlet, a dew point measurement of the supply air was used along with the dry bulb temperature measurement. A variable frequency driven booster fan was controlled downstream of the nozzles to make up for any pressure drop occurring in the duct configuration of the rooftop unit and through the nozzles.

2.3.9 Data Acquisition System

A National Instruments embedded real time controller (NI-CRIO 9024) was used for data collection and control. Several modules having different functionalities were used with the real time controller to facilitate and perform data collection and control operations as summarized in Table 3.

Table 3. Data acquisition system functionalities.

Modules	Functionality
NI 9213	16-ch thermocouple input
NI 9205	16-ch differential analog input
NI 9265	4-ch analog output
NI 9870	4-ch RS 232 serial input
NI 9474	8-ch sourcing digital output

2.3.10 Indoor Blower and Outdoor Fan Control

The outdoor fan was a variable speed ECM motor driven fan that works on Pulse Width Modulation (PWM) signal input. A black box controller (model: EVO/ECM-VCU) from Evolution Controls was used to control the speed of the condenser fan by varying the duty cycle of the PWM signal. The speed of the indoor blower with a variable speed ECM motor was controlled by a built-in Lennox Prodigy controller.

2.3.11 Heat Exchanger Fouling

The fouling conditions of the heat exchangers were simulated by reducing the air flow across the heat exchangers. On the evaporator side, the target air flow for a given fouling level was achieved by running the nozzle box booster fan at a lower frequency along with

a reduced speed of the indoor blower. On the condenser side, the fouling scenario was achieved by running the outdoor fan at a lower speed.

2.4 Data Analysis and Uncertainty

2.4.1 Data Analysis

The condenser outlet subcooling is calculated as the difference between the temperature of the refrigerant leaving the condenser and the saturated condensing temperature at the exit pressure. The temperature of the refrigerant leaving the condenser was measured using a T-type thermocouple. However, since the micro-channel condenser has only a single pass between the inlet and the outlet headers and doesn't have any return bends, a direct measurement of the condensing temperature using a surface mounted T-type thermocouple was impossible. Hence, a high side pressure measurement at the outlet of condenser was employed along with thermodynamic properties to determine condensing temperature.

$$T_{sc} = T_{sat,cond} - T_{out,ref,cond} \tag{2.3}$$

The evaporator outlet superheat is calculated as the difference between the temperature of the refrigerant leaving the evaporator and the saturated evaporating temperature. The temperature of the liquid leaving the evaporator was measured using a T-type thermocouple at the exit of the evaporator and the saturated evaporating temperature was measured at the inlet of the evaporator as the refrigerant entering the evaporator is a two-phase mixture.

$$T_{sh} = T_{out,ref,evap} - T_{sat,evap} \tag{2.4}$$

The compressor discharge superheat is calculated as the difference between the temperature of the refrigerant leaving the compressor and the condensing temperature based on the compressor discharge pressure. But since the pressure drop across the micro-

channel condenser is typically small compared to a fin-tube condenser, condenser outlet pressure was used in place of the compressor discharge pressure.

$$T_{dsh} = T_{out,ref,comp} - T_{sat,cond} \tag{2.5}$$

The quality of the refrigerant entering the evaporator is obtained by using the pressure and temperature of the refrigerant exiting the condenser to obtain the enthalpy based on thermodynamic properties and assuming an isenthalpic expansion process along with the inlet evaporator refrigerant temperature. However, in case of a two-phase refrigerant mixture exiting the condenser, the refrigerant enthalpy and quality could not be calculated. In order to calculate the cooling capacity, the refrigerant enthalpies were calculated based on thermodynamic property relations using CoolProp [10]. The refrigerant enthalpies were calculated using refrigerant pressure and temperature measurements along different locations of the refrigerant cycle.

The refrigerant side cooling capacity is calculated as,

$$\dot{Q}_{cooling,ref} = \dot{m}_{ref} \left(h_{out,ref,evap} - h_{in,ref,evap}\right) \tag{2.6}$$

It should be noted that when two-phase occurs at the exit of the condenser, the refrigerant side cooling capacity cannot be calculated as the mass flow rate of the two-phase mixture could not be measured and the quality at the inlet of the evaporator could not be calculated. The airflow across the condenser coil is not measured and was estimated based on an energy balance as shown below,

$$\dot{m}_{a,cond} = \frac{\dot{m}_{ref} \left(h_{in,ref,cond} - h_{out,ref,cond}\right) + \dot{W}_{cond,fan}}{c_{pa,cond} \left(T_{out,air,cond} - T_{in,air,cond}\right)} \tag{2.7}$$

The dry bulb temperature of the air entering and leaving the condenser was measured using T-type thermocouples whereas the refrigerant enthalpies were calculated using thermodynamic property relations based on refrigerant temperature and pressure measurements. However in cases when the condenser subcooling is less than 2K, the refrigerant mass flow rate is not reliable and hence the condenser air flow rate for these points could not be calculated.

2.4.2 Uncertainty

The quality of the experimental test results depends on the uncertainty. In many cases, certain quantities are not directly measured but are calculated as a function of other directly measured quantities. The uncertainty in these measured quantities will affect the accuracy of the derived quantities. The uncertainty propagation of these derived quantities can be calculated using the Kline and McClintock method in EES, which can be expressed as,

$$\omega_A = \left[\sum_{i=1}^{j} \left(\frac{\partial A}{\partial Z_i} \omega_{zi} \right)^2 \right]^{1/2} \tag{2.8}$$

where ω_A is the uncertainty in the calculated variable A, Z_i is one of the measured variables which impacts the calculated variable and ω_{zi} is the uncertainty associated with that measured variable. The average uncertainties of derived variables are shown Table 4.

Table 4. Uncertainties of derived quantities.

Derived quantities	Uncertainty (absolute or relative)
Condenser outlet subcooling	±1.0 °C
Evaporator outlet superheat	±1.4 °C
Compressor discharge superheat	±1.0 °C

Evaporator inlet quality	±0.011
Refrigerant side cooling capacity	±1.2 %
Condenser air flow rate	±7.1 %
Air side cooling capacity (based on RH sensors)	±8.01%
Air side cooling capacity (based on dew point sensors)	±6.0%

2.5 Open Laboratory Training

2.5.1 Motivation

In previous studies, virtual sensors for rooftop applications have required extensive training data obtained over a wide range of conditions in order to determine the required empirical parameters. For instance, training of the virtual refrigerant charge sensor has required varying the charge level of the system for a range of different outdoor and indoor test conditions. Previously this data has been obtained through extensive testing within psychrometric chambers. This is a big obstacle for equipment manufacturers considering the range of different models that they support and the high cost of instrumenting and testing equipment using psychrometric chambers.

In order to significantly reduce the cost of training virtual refrigerant charge (VRC) sensors, we propose to obtain data in an open space and artificially increase the condensing and lower evaporating temperatures by changing the air flows across the heat exchangers. It is still necessary to vary the refrigerant charge over the range of interest. However, the number of data points and time required for testing can be significantly reduced. Furthermore, the overall training cost is significantly reduced by eliminating the

requirement for testing in psychrometric chambers that are heavily utilized for other purposes. For virtual capacity and compressor power sensors, it is proposed to utilize manufacturers compressor maps as described in Chapter 3 to avoid the need for model training.

2.5.2 Methodology for Adjusting Operating Conditions

Figure 4 illustrates the concept of artificially changing the condensing and evaporating pressures (and temperatures) on a pressure – enthalpy diagram for a typical vapor-compression refrigeration cycle. At different operating conditions, the evaporator and condenser saturation pressures will reach equilibrium conditions that depend on both the ambient conditions and the ability of the heat exchangers to transfer heat. Thus, higher condenser air inlet temperatures lead to high condensing temperatures, while lower evaporator air inlet temperatures give lower evaporation temperatures. However, these same variations can be achieved in an open laboratory with constant air inlet temperatures by varying the air flow rates (and therefore the heat transfer rates) through the condenser and evaporator. Lower condenser airflow leads to higher condensing temperature (and pressure), while lower evaporator pressure (and temperature) results from a lower evaporator airflow rate.

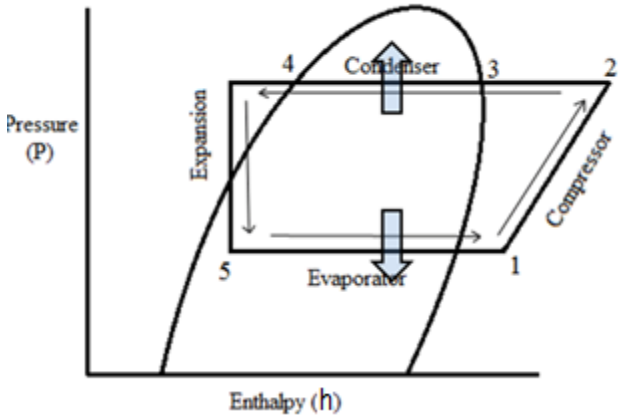

Figure 4. Depiction of a vapor compression cycle condensing and evaporator pressure changes due to variable air flow on a P-h diagram.

Adjustments in air flow rate can be achieved in different ways depending on the system configuration. In the case of constant speed fans, a volume control damper could be installed downstream of the fans to adjust the flow resistance and affect the flow. For constant torque fans that use variable frequency drives to adjust the fan speed, a control input in the form of frequency can be used to directly change air flow without the need for dampers. In the case of ECM motor driven fans that use Pulse Width Modulation (PWM) signals to control the speed of the fans, a control input in the form of a PWM duty cycle can be directly used to change the speed of the fans and hence varying the air flow. This approach was employed for both the evaporator and condenser air flow adjustments in this study.

2.5.3 Open Lab Experimental Conditions

The rooftop unit was made to run in an open lab space in Herrick labs and data at different charge levels, condensing temperatures, and evaporating temperatures were collected in the open laboratory for the virtual refrigerant charge sensor models. This data was used to

train the virtual refrigerant charge sensor in Chapter 4. Table 5 shows the different operating conditions for the open lab testing of the rooftop unit.

Table 5. Open lab test matrix for the RTU.

Charge level [% of nominal charge level]	Compressor stage of operation	Indoor blower PWM duty cycle [%]	Outdoor fan PWM duty cycle [%]
60% - 120%	First	60%; 40%; 20%	70%; 50%; 30%
60% - 120%	Second	90%; 70%; 50%	100%; 80%; 60%

The charge level was varied from 60%-120% of the nominal charge in increments of 10% of the nominal charge for both stages of operation. The indoor blower and the outdoor fan were controlled by control inputs in the form of PWM duty cycle to control their speed.

2.6 Psychrometric Room Evaluation

The rooftop unit was installed in the psychrometric chambers of the Herrick laboratories to simulate different indoor and outdoor ambient conditions.

2.6.1 Motivation

The accuracy of the virtual charge, capacity, and compressor power sensors were evaluated over a wide range of operating conditions that a rooftop unit would typically run to ensure that the virtual sensor readings are reliable. In order to perform this evaluation, the rooftop unit was installed in the psychrometric chambers and the indoor and outdoor room conditions were controlled to simulate different operating conditions of the rooftop unit.

2.6.2 Room setup

The rooftop unit was installed in the psychrometric rooms as shown in Figure 5.

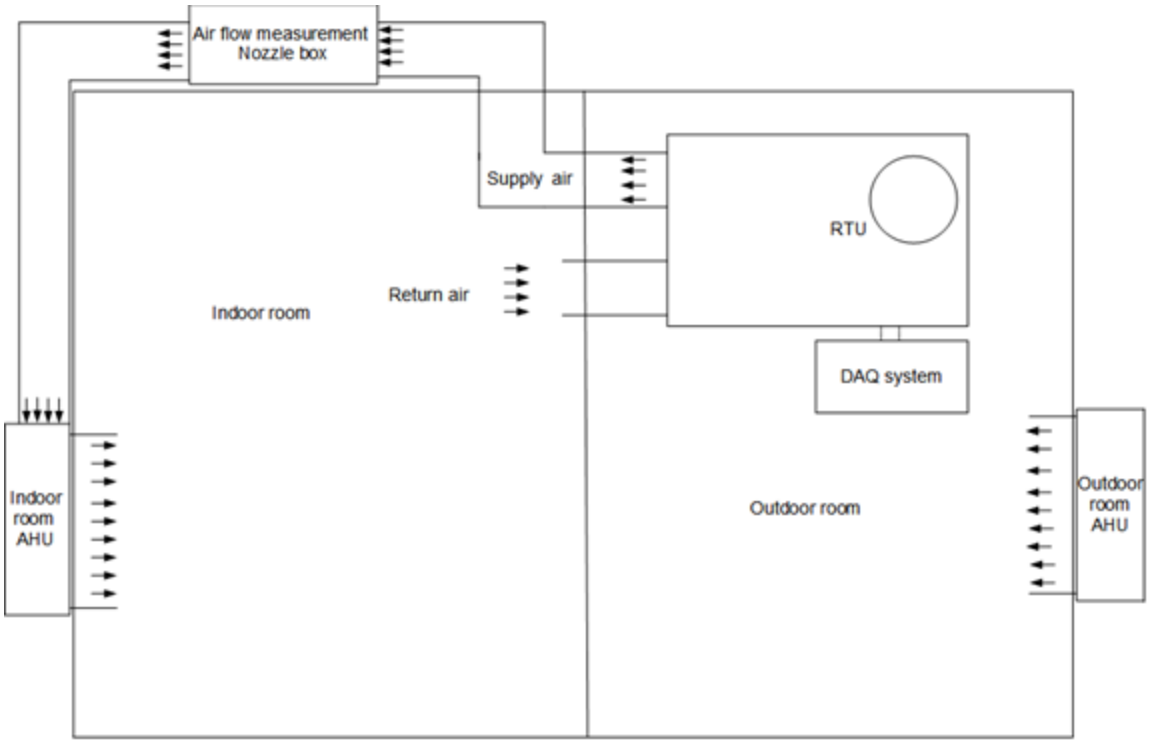

Figure 5. Psychrometric room setup of the RTU.

The rooftop unit was installed with air ducts connected to the supply and return air streams as shown in Figure 6. On the supply air side, the air ducts connected the rooftop unit to the air flow measurement nozzle box enabling measurement of the supply air flow rate. The nozzle box has a booster fan downstream of the measurement nozzles, which is controlled using a variable frequency drive (VFD) to overcome the pressure drop occurring in the air duct. On the return air side, ducts from the bottom of the mixing chamber connect the rooftop unit to the indoor room. The data acquisition device was installed next to the rooftop unit and was connected to the monitoring system outside the rooms via the building Local Area Network (LAN).

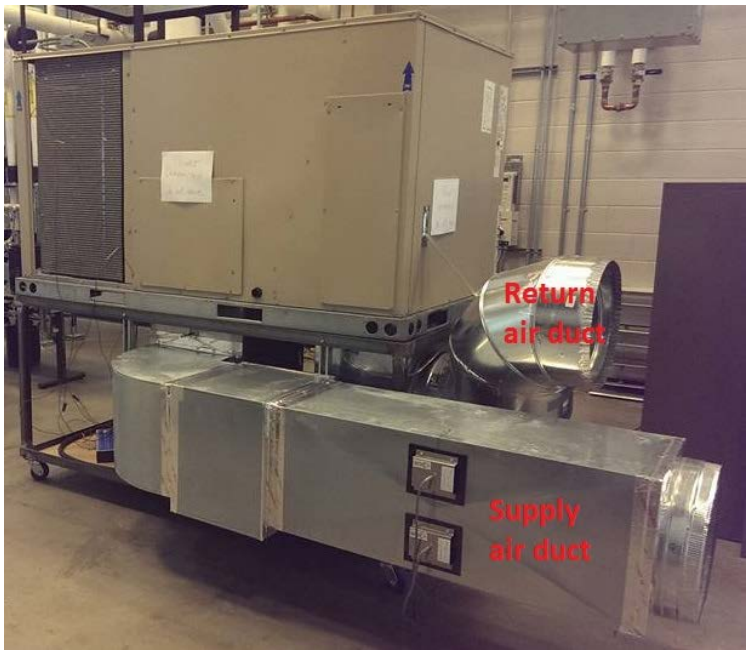

Figure 6. RTU duct configuration.

2.6.3 Evaluation Matrix

The virtual sensors were evaluated over a wide range of steady-state operating conditions using data obtained in the psychrometric chambers. The ranges of test operating conditions are shown in Table 6. The charge level was varied from 60% - 120% of normal charge at 10% increments for both stages of the operation of the rooftop unit. The indoor conditions were kept constant at 80°F and 50% relative humidity, while the outdoor air temperature was varied from 67°F to 108°F. The indoor and outdoor air flow rates of the unit were controlled to simulate fouling conditions for both evaporator and condenser. The three different air flow levels chosen to evaluate the virtual sensors are representative of conditions that could typically occur in a fouled condenser or evaporator. The total number of test points for evaluation of the virtual sensors was 215.

Table 6. Evaluation test conditions for the virtual sensors.

Charge level [% of nominal charge level]	Compressor stage of operation	Ambient Conditions [°F]	Indoor unit air flow levels [% of nominal air flow level]	Outdoor unit air flow levels [% of nominal air flow level]
60% - 120%	First	67; 82; 95	100%;83%;60%	100%;50%;30%
60% - 120%	Second	82; 95; 108	100%;83%;63%	100%;60%;30%

CHAPTER 3. EVALUATING VIRTUAL SENSOR ACCURACY AND COSTS

3.1 Introduction

This chapter presents detailed evaluations of the accuracies of the virtual sensors and provides an initial assessment of implementation costs for an embedded application. For virtual refrigerant charge, the accuracy of different model forms investigated using experimental data for the rooftop unit with micro-channel condenser. Section 3.2 explains the different model forms of the virtual refrigerant charge sensor used along with the model evaluation approach used to evaluate these virtual sensor models and their results. Section 3.3 and 3.4 focuses on virtual compressor power and virtual cooling capacity sensor performance results. Section 3.5 presents cost estimates for these virtual sensors implemented within manufactured RTUs as an embedded system and also provides estimates of cost savings compared to using direct sensor measurements.

3.2 Virtual Refrigerant Charge Sensor Model Descriptions

A number of different virtual refrigerant charge sensor models were investigated to determine the most appropriate model form for the rooftop unit with micro-channel condenser. The best model was determined by comparing the RMSE of the different virtual refrigerant charge sensor model forms over the range of charge levels of interest.

All the virtual refrigerant charge sensor models are gray-box models that correlate the amount of normalized refrigerant charge with parameters such as evaporator superheat,

condenser subcooling, compressor discharge superheat and evaporator inlet quality relative to their values when the unit is properly charged at a rating condition. Previous studies have shown that these quantities have a significant sensitivity to charge level [11, 12]. It should also be noted that all these models were developed based on the assumption that the rooftop unit is running in steady-state operating conditions.

3.2.1 Description of Different Alternative Model Forms

Virtual Refrigerant Charge Sensor Model I

VRC sensor model I was developed by Li and Braun [11] and correlates the amount of normalized refrigerant charge in the unit to evaporator superheat and condenser subcooling with the following mathematical form,

$$\frac{m_{charge,actual}}{m_{charge,rated}} = 1 + k_{sc}(\Delta T_{sc} - \Delta T_{sc,rated}) + k_{sh}(\Delta T_{sh} - \Delta T_{sh,rated}) \tag{3.1}$$

where $m_{charge,actual}$ is the mass of actual refrigerant in the system, $m_{charge,rated}$ is the mass of nominal (rated) refrigerant, k_{sc} is the empirical subcooling parameter, k_{sh} is the empirical evaporator superheat parameter, ΔT_{sc}, ΔT_{sh} are the condenser subcooling and evaporator superheat at the operating conditions and $\Delta T_{sc,rated}$, $\Delta T_{sh,rated}$ are the condenser subcooling and evaporator superheat at the rating condition with the nominal charge.

Virtual Refrigerant Charge Sensor Model II

The VRC sensor model II includes the inlet quality of the evaporator in addition to the condenser subcooling and evaporator superheat to estimate the amount of refrigerant charge and was developed by Kim and Braun [12]. The quality of the refrigerant entering the evaporator is calculated from the measurements exiting the condenser along with the

inlet temperature of the evaporator assuming an isenthalpic expansion process. The form of the virtual charge sensor model is

$$\frac{m_{charge,actual}}{m_{charge,rated}} = 1 + k_{sc}(\Delta T_{sc} - \Delta T_{sc,rated}) + k_{sh}(\Delta T_{sh} - \Delta T_{sh,rated}) + k_x(x_{evap,in} - x_{evap,in,rated}) \quad (3.2)$$

where k_x is the empirical parameter for inlet quality of the evaporator, $x_{evap,in}$ is the inlet quality of the evaporator at the operating conditions and $x_{evap,in,rated}$ is the inlet quality of the evaporator at the rated condition with the nominal charge.

Virtual Refrigerant Charge Sensor Model III

This VRC sensor model III replaces evaporator superheat in model II with compressor discharge superheat. The compressor discharge superheat is defined as the difference between the temperature of the refrigerant leaving the compressor and the saturated condensing temperature. The following model form is employed,

$$\frac{m_{charge,actual}}{m_{charge,rated}} = 1 + k_{sc}(\Delta T_{sc} - \Delta T_{sc,rated}) + k_{dsh}(\Delta T_{dsh} - \Delta T_{dsh,rated}) + k_x(x_{evap,in} - x_{evap,in,rated}) \quad (3.3)$$

where k_{dsh} is an empirical parameter related to the discharge superheat of the compressor, ΔT_{dsh} is the compressor discharge superheat at the operating conditions and $\Delta T_{dsh,rated}$ is the discharge superheat of the compressor at the rated condition with the nominal charge.

Virtual Refrigerant Charge Sensor Model IV

This VRC sensor model correlates the normalized amount of refrigerant charge in the unit to condenser subcooling, evaporator superheat, compressor discharge superheat and inlet quality of the evaporator and was developed by Kim and Braun [3]. This VRC model is of the form,

$$\frac{m_{charge,actual}}{m_{charge,rated}} = 1 + k_{sc}(\Delta T_{sc} - \Delta T_{sc,rated}) + k_{dsh}(\Delta T_{dsh} - \Delta T_{dsh,rated}) + k_{x}(x_{evap,in} - x_{evap,in,rated}) + k_{sh}(\Delta T_{sh} - \Delta T_{sh,rated}) \quad (3.4)$$

3.2.2 Model Evaluation Approach

The different rated constants in the virtual refrigerant charge sensor models such as $\Delta T_{sc,rated}$, $\Delta T_{dsh,rated}$, $x_{evap,in,rated}$, $\Delta T_{sh,rated}$ and $m_{charge,rated}$ can be readily estimated from manufacturer's data or from test data. The rated conditions should be determined in the absence of any faults in the system and in steady-state operating conditions of the unit at a set of given indoor and outdoor conditions. For this study the rated condition is chosen as the AHRI 210/240 performance rating conditions for a rooftop unit with indoor conditions of 80°F/67°F dry bulb/wet bulb temperature and outdoor conditions of 82°F/65°F dry bulb/wet bulb temperature.

The empirical parameters k_{sc} , k_{dsh} , k_{x} and k_{sh} of the virtual refrigerant charge sensor models are learned by least squares regression applied to data. In order to compare the accuracy of the different model forms, the empirical coefficients were estimated based on the experimental data obtained from psychrometric room testing for the conditions shown in Table 6. The RMSE of the different VRC sensor models were compared over the entire range of interest and the model with the minimum RMSE is chosen as the best model. The accuracy of open laboratory testing was considered for the final model form in Chapter 4.

3.2.3 Model Results and Discussion

Virtual Refrigerant Charge Sensor Model I

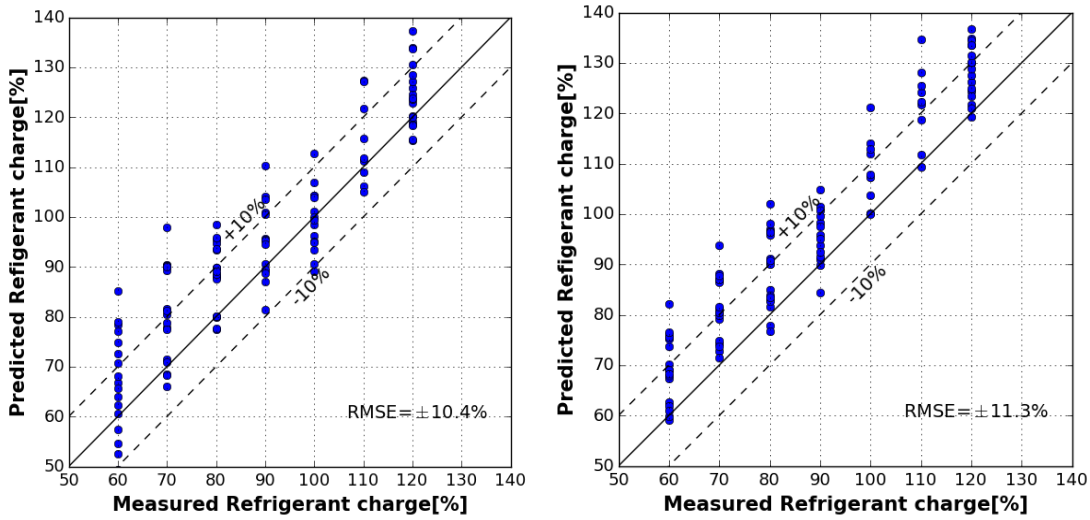

Figure 7. VRC model I accuracy for (a) first stage of operation and (b) second stage of operation.

Figure 7 shows the performance of the virtual refrigerant charge sensor with separate coefficients trained for each individual stage of operation. The first stage sensor has an RMSE of ±10.4% while the second stage sensor has an RMSE of ±11.3%. It could also be seen that this model has biased charge predictions especially for the second stage of operation. The VRC sensor model was also be trained with a single set of coefficients for both the stages of operation with results shown in Figure 8. In this case, the RMSE of the combined model for both stages of operation is ±11.4%.

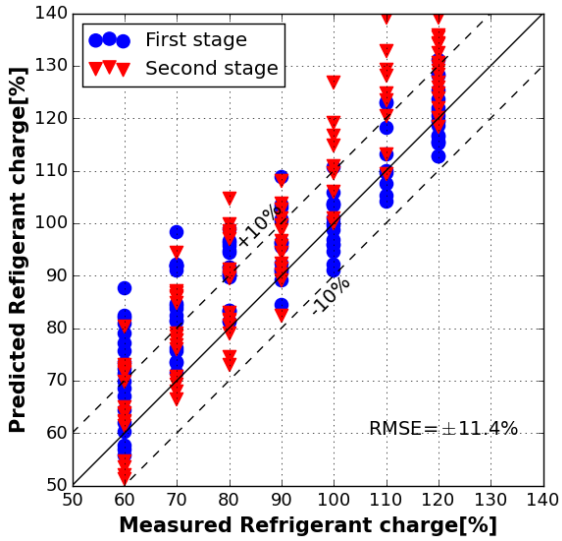

Figure 8. VRC model I accuracy for both stages of operation using a single set of coefficients.

Virtual Refrigerant Charge Sensor Model II

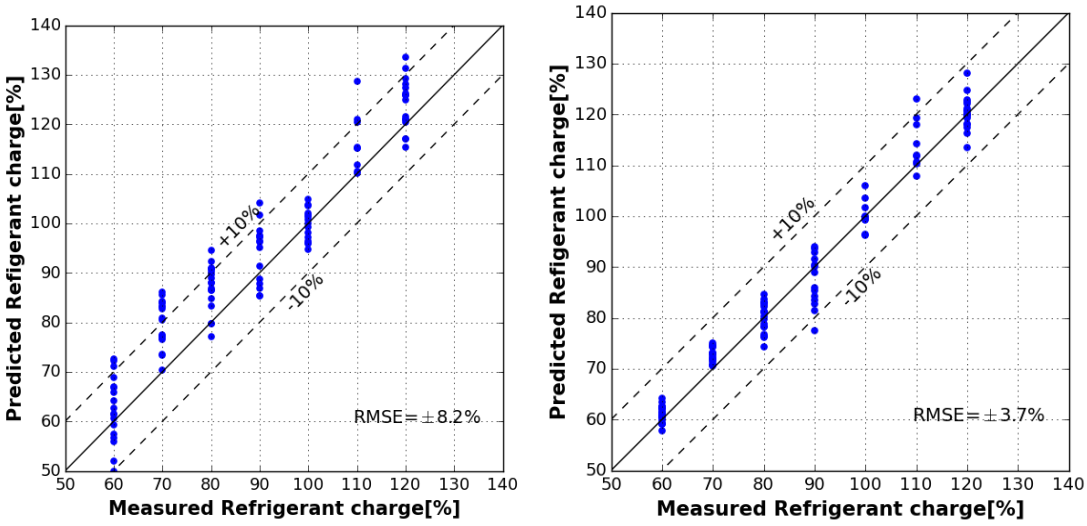

Figure 9. VRC model II accuracy for (a) first stage of operation and (b) second stage of operation.

Figure 9 shows the performance of the virtual refrigerant charge sensor II with separate coefficients trained for each individual stage of operation. The first stage sensor has an RMSE of ±8.2% while the second stage sensor has an RMSE of ±3.7%. It should also be

noted that the biases in the predictions are significantly reduced in this VRC model compared to VRC model I. Also, the VRC sensor model was trained with a single set of coefficients for both the stages of operation with results shown in Figure 10. In this case, the RMSE of the combined model for both stages of operation is ±8.0%. While a few test points have prediction errors greater than the 10% error bounds, most of them are within ±10%.

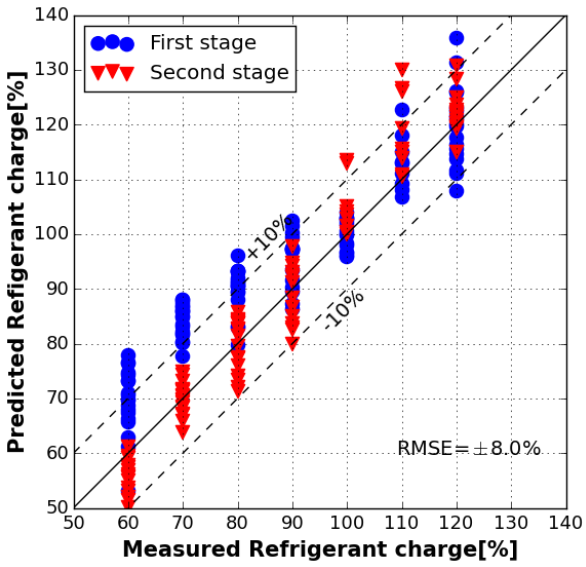

Figure 10. VRC model II accuracy for both stages of operation using a single set of coefficients.

It can be seen that the performance of the VRC model II is better than that of VRC model I with lower RSME.

Virtual Refrigerant Charge Sensor Model III

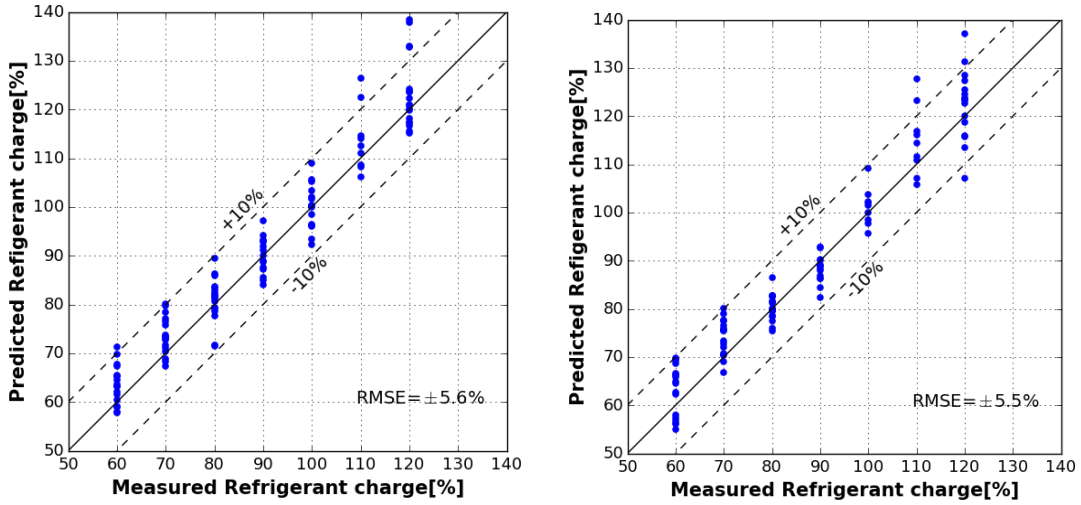

Figure 11. VRC model III accuracy for (a) first stage of operation and (b) second stage of operation.

VRC model III uses compressor discharge superheat in place of evaporator superheat in VRC model II. Figure 11 shows the performance of the virtual refrigerant charge sensor with separate coefficients trained for each individual stage of operation. The first stage sensor has an RMSE of ±5.6% while the second stage sensor has an RMSE of ±5.5%. The VRC sensor model trained with a single set of coefficients for both the stages of operation gives the results shown in Figure 12. In this case, the RMSE of the combined model for both stages of operation is ±6.6%. The performance of this VRC sensor is particularly good in the range of 90%-110% of the nominal charge. Qualitatively this is a good behavior and should correctly identify refrigerant charge faults when the amount of charge is less than 90% and greater than 120% of the nominal charge.

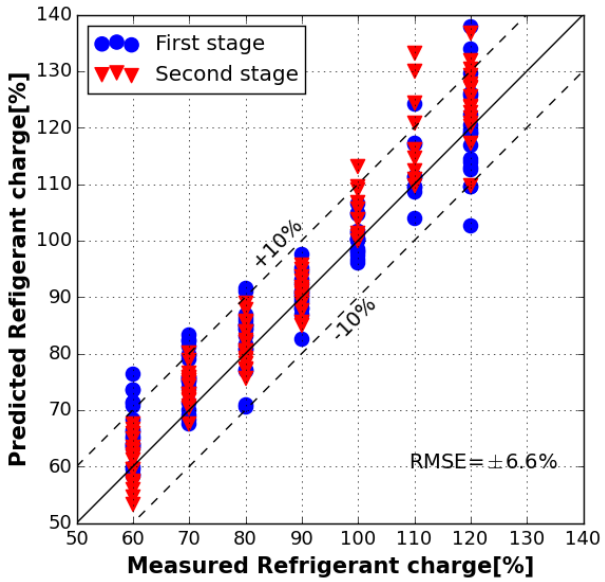

Figure 12. VRC model III accuracy for both stages of operation using a single set of coefficients.

Virtual Refrigerant Charge Sensor Model IV

This model correlates the amount of normalized refrigerant charge to condenser subcooling, evaporator superheat, compressor discharge superheat and inlet quality of the evaporator as explained in section 3.2.1. During the process of evaluating this model form, issues of multicollinearity were identified and the evaporator superheat and compressor discharge superheat were found to be highly correlated as shown in the Pearson product-moment correlation matrix in Table 7. The Pearson product-moment correlation coefficient ρ_{xy} between two variables x and y is calculated as,

$$\rho_{xy} = \frac{\mathrm{cov}(x,y)}{\sigma_x \sigma_y} \tag{3.5}$$

where $\mathrm{cov}(x,y)$ is the covariance of the two variables and σ_x, σ_y is the standard deviation of the variables x and y. The value of this coefficient ranges from +1 to -1 indicating strong positive correlation to strong negative correlation.

Table 7. Pearson correlation matrix.

Variables	Evaporator superheat	Condenser subcooling	Compressor discharge superheat	Evaporator inlet quality
Evaporator superheat	1.0	-0.78	0.96	0.62
Condenser subcooling	-0.78	1.0	-0.76	-0.74
Compressor discharge superheat	0.96	-0.76	1.0	0.68
Evaporator inlet quality	0.62	-0.74	0.68	1.0

As shown in Table 7, the correlation between evaporator superheat and the compressor discharge superheat variables in this VRC sensor model is 0.96 which indicates very high positive correlation. Hence, this model has significant multicollinearity which would cause the variance of the model and the confidence interval of the coefficients estimated to be inflated resulting in any inference made from the model to be unreliable. Hence no further evaluations are presented for this model.

3.3 Virtual Compressor Power Sensor

The virtual compressor power sensor uses the standard AHRI compressor map that is typically available from the manufacturer. The standard map correlates the compressor input power to saturated condensing and evaporating temperature using a 10-coefficient polynomial equation as shown below [13],

$$\dot{W}_{rated} = c_1 + c_2 T_e + c_3 T_c + c_4 T_e^{\,2} + c_5 T_e T_c + c_6 T_c^2 + c_7 T_e^3 + c_8 T_c T_e^2 + c_9 T_e T_c^2 + c_{10} T_c^3 \quad (3.6)$$

where $\dot{W}_{rated}$ is the compressor input power consumption, T_e is the saturation temperature corresponding to the compressor inlet (suction) pressure, T_c is the saturation temperature corresponding to the compressor outlet (discharge) pressure and c_1 - c_{10} are the empirical coefficients. Since these coefficients are readily available from the compressor manufacturer, there are no training requirements associated with this sensor. It should be noted that in this study since the compressor used was a dual stage scroll compressor, individual compressor maps were used for the respective stages of operation.

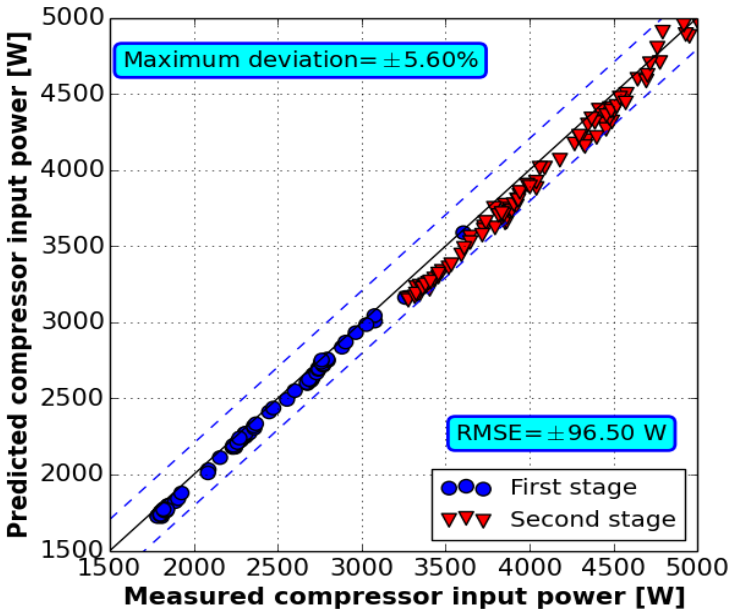

Figure 13. Virtual compressor power sensor performance.

Figure 13 shows the measured input compressor power compared to predicted compressor power of the unit based on the virtual compressor power sensor. The AHRI compressor map works very well for the entire data set with a maximum deviation of ±5.6% with a RMSE of ±96.5 W. There is a small bias with the model slightly under predicting the power compared to the measurements.

3.4 Virtual Cooling Capacity Sensor

The cooling capacity of a rooftop unit when operating at steady state is given by

$$\dot{Q}_{cooling,ref} = \dot{m}_{ref} (h_{out,ref,evap} - h_{in,ref,evap}) \tag{3.7}$$

The virtual cooling capacity is obtained by using a virtual refrigerant mass flow rate in place of the actual flow rate [13] such that

$$\dot{Q}_{cooling,ref,virtual} = \dot{m}_{ref,virtual} (h_{out,ref,evap} - h_{in,ref,evap}) \tag{3.8}$$

The virtual refrigerant mass flow rate sensor uses the AHRI based compressor map that correlates the refrigerant mass flow rate to the saturated condensing and evaporator temperatures using a third degree polynomial equation as shown below,

$$\dot{m}_{map} = d_1 + d_2 T_e + d_3 T_c + d_4 T_e^2 + d_5 T_e T_c + d_6 T_c^2 + d_7 T_e^3 + d_8 T_c T_e^2 + d_9 T_e T_c^2 + d_{10} T_c^3 \quad (3.9)$$

where $\dot{m}_{map}$ is the compressor map based flow rate, T_e is the saturation temperature corresponding to the compressor inlet (suction) pressure, T_c is the saturation temperature corresponding to the compressor outlet (discharge) pressure and d_1 - d_{10} are the empirical coefficients. Since these coefficients are readily available from the compressor manufacturer there are no training requirements associated with this sensor. Also, it should be noted that in this study since the compressor used was a dual stage scroll compressor, individual compressor maps was used for the respective stages.

The map based flow rate is then adjusted for the inlet superheat of the compressor based on the Rice correlation [14] as follows,

$$\frac{\dot{m}_{new}}{\dot{m}_{map}} = 1 + F\left(\frac{\rho_{new}}{\rho_{map}} - 1\right) \quad (3.10)$$

where $\dot{m}_{new}$ is the corrected refrigerant mass flow rate at the operating condition, $\dot{m}_{map}$ is the compressor map based flow rate, F is a correction factor to account for suction gas heating within a hermetic compressor which is assumed to be 0.75, ρ_{new} is the suction density at the operating condition and ρ_{map} is the suction density at the map based superheat.

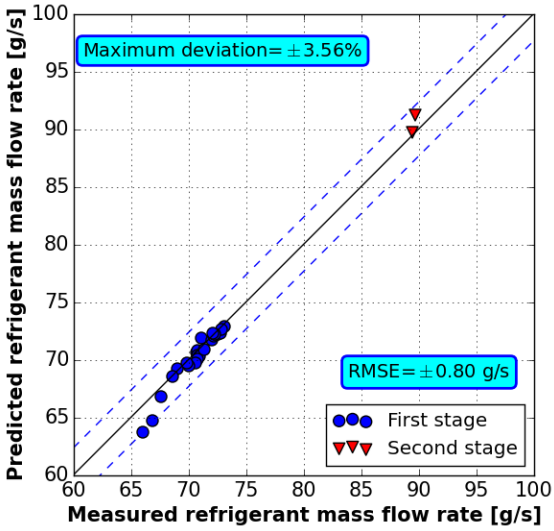

Figure 14. Virtual refrigerant mass flow rate sensor performance.

Figure 14 shows comparisons between measured and predicted refrigerant mass flow rate based on the virtual refrigerant mass flow rate sensor. The installed mass-flow meter does not provide reliable measurements under conditions with a two-phase mixture. Hence, points having a condenser subcooling of less than 1.5 K were filtered out and not included in the comparison. Furthermore, the installed micro-motion mass flow meter did not have the proper range for the application and saturated at 90 g/s of refrigerant flow rate. Since most of the second stage operation had values of refrigerant mass flow rate higher than 90 g/s those points were also filtered out from the validation plot. It can be seen that the virtual refrigerant mass flow sensor based on AHRI map works well for both stages of operation with a RMSE of ±0.8 g/s and a maximum deviation of ±3.56%. Figure 15 compares the measured cooling capacity based on the installed mass flow meter and the predicted cooling capacity based on the virtual cooling capacity sensor.

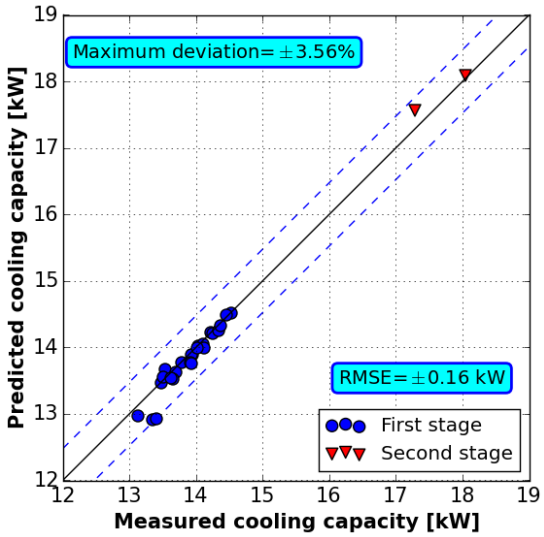

Figure 15. Virtual cooling capacity sensor performance relative to refrigerant-side capacity.

Here again it can be seen that the virtual cooling capacity sensor works pretty well with a maximum deviation of ±3.56% and a RMSE of ±0.16 kW.

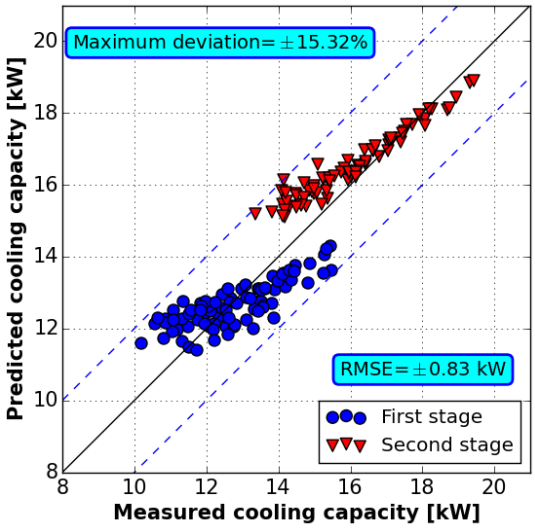

Figure 16. Virtual cooling capacity sensor performance relative to air-side cooling capacity.

Since there were not many reliable refrigerant-side capacity measurements, virtual cooling capacity sensor capacity predictions relative to measured air-side cooling capacity are shown in Figure 16. The differences are significantly larger than those associated with the virtual cooling capacity and refrigerant-side capacity comparisons. This could be because of the higher uncertainty in accurately measuring the air-side capacity as shown in Table 4. However the RMSE is reasonably good at around ±0.83 kW while the maximum deviation is ±15.32%.

3.5 Virtual Sensor Implementation Costs and Savings Relative to Direct Measurements

The cost of implementing virtual sensors within manufactured RTUs is an important consideration. It is particularly important that the costs of the virtual sensor inputs are less than the cost of measuring each quantity directly. Ideally, the virtual compressor power and mass flow sensors (AHRI) would use compressor suction and discharge pressure along with compressor inlet temperature as inputs. These pressures would be used along with thermodynamic property relations to estimate saturation suction and discharge temperatures. The virtual capacity sensor also requires knowledge of the enthalpy entering the evaporator. The refrigerant enthalpy entering the evaporator is practically the same as the enthalpy leaving the condenser. If refrigerant pressure drop across the condenser is small (a good assumption for micro-channel condensers) then compressor discharge temperature and the refrigerant temperature leaving the condenser can be used along with thermodynamic properties to obtain a good estimate of the enthalpy entering the evaporator. The virtual charge sensor considered in this study requires condensing temperature (or pressure), liquid temperature leaving the condenser, evaporating temperature (or pressure), and compressor discharge temperature. The compressor discharge pressure can be used to

estimate the condensing pressure. The evaporating temperature can either be estimated using the compressor suction pressure (when evaporator superheat is needed) or using a surface mounted temperature at the inlet to the evaporator (when inlet quality is needed). As a result of these considerations, the following sensors shown in Table 8 are believed to be ideal as inputs for the 3 virtual sensors considered in this study.

Table 8. Ideal sensor inputs to virtual sensors.

Ideal sensor inputs	Virtual sensors
Compressor suction pressure	Virtual compressor power and cooling capacity sensors
Compressor discharge pressure	Virtual charge, compressor power and cooling capacity sensors
Compressor discharge temperature	Virtual charge sensor
Condenser outlet temperature	Virtual charge and cooling capacity sensors
Evaporator inlet temperature	Virtual charge sensor
Evaporator outlet temperature	Virtual charge and cooling capacity sensors

High volume OEM costs for temperatures sensors are around $5 per sensor and $20 for pressure sensors [15]. Hence, the total cost of these required sensors would be approximately $60. If an additional pressure sensor were needed at the outlet of the condenser to get a more accurate subcooling measurement for fin-tube condensers (due to larger refrigerant pressure drops for this type of condenser), then the total sensor cost would be closer to $80. It should be possible to implement the virtual sensor models within the existing RTU controller. However, if an additional microprocessor or enhanced micro-

controller were needed then this could add up to $40 to the cost of the virtual sensors. Therefore, the virtual sensor costs would be in the range of $60 to $120 for an embedded RTU application. This cost structure is presented in Table 9.

Table 9. Typical cost breakdown of virtual sensor implementation.

Typical OEM sensor costs for temperature sensor	~$5
Typical OEM sensor costs for pressure sensor	~$20
Total cost of ideal virtual sensor inputs	~$60
Total cost of virtual sensor inputs with condenser outlet pressure measurement	~$80
Virtual sensor implementation using existing RTU micro-controller	~$80
Virtual sensor implementation using additional micro-controller.	~$100

It is interesting to compare the virtual sensor costs to costs required for direct measurements. It is not possible to implement a direct measurement of refrigerant charge on board an RTU. Therefore, there is no baseline for comparison. On the other hand, power transducers are widely available but are relatively expensive. Retail prices for an appropriate power transducer are about $500 per unit [16]. Assuming that OEM prices in quantity are 70% of retail costs, a reasonable price might be $350 per unit. Direct measurement of refrigerant flow is extremely expensive (e.g. > $4000 per sensor) and not practical. An alternative would be to measure air- side capacity using a hot-wire anemometer for velocity along with inlet and outlet temperatures and humidity. The

estimated cost of this approach would be $350 per RTU. However, the accuracy could be poor due to the use of single-point measurements of velocity, temperature, and humidity and the well-known difficulty in reliably measuring humidity. Even so, the cost of $700 per RTU for on-board power and capacity would be difficult to justify. This cost structure is presented in Table 10.

Table 10. Typical cost estimate for direct sensor measurements.

Cost of power transducer (70% of the retail costs)	~$350
Cost of directly measuring air-side cooling capacity	~$350
Cost of measuring the refrigerant charge	Not possible
Total cost of direct measurements (for compressor power and capacity only)	~$700

By comparing the virtual sensor implementation cost in Table 9 and the cost of direct measurements in Table 10, it is clear that the virtual sensor cost of $100 would be more attractive and provides the additional output of virtual charge along with power and capacity.

CHAPTER 4. MINIMIZING TRAINING COSTS FOR THE VRC SENSOR

This chapter focuses on minimizing the training requirements for the virtual refrigerant charge sensor using open lab training data (see section 4.1) with an algorithm that minimizes the number of training points (see section 4.2 and 4.3). Evaluation of how well the open lab training methodology works for the virtual refrigerant charge sensor is also presented in section 4.4.

4.1 Opportunities for Reducing Engineering Costs Using Open Lab Training

One of the main drawbacks of the VRC sensor has been the requirement for extensive training data obtained using psychrometric chambers. This involved varying the charge level for a range of different outdoor and indoor conditions. From a manufacturer's perspective, this time in the psychrometric chambers is expensive and would prohibit the VRC implementation. Therefore, it is advantageous to develop an alternative VRC training methodology that uses open lab training data to learn the VRC model as described in section 2.5.

In addition to eliminating the need for expensive setups in psychrometric chambers, the process of running through different operating conditions in an open laboratory environment could be automated leading to additional cost reductions. Furthermore, there is potential for applying this automated training approach to units installed in the field.

4.2 Algorithm for Minimizing the Number of Training Data Points

For the case considered in this thesis, the total number of open lab data points available for training is 35 for each stage (70 total). The specific conditions for this test data are shown in Table C.1. and Table C.2. It can be seen that the charge level was varied from 60% to 120% of the nominal charge level in steps of 10% increment. At each charge level, the total number of combinations of evaporator and condenser fan PWM duty cycle variations was chosen to be 5. These combinations were chosen so as to include three out of the four combinations of upper and lower fan settings (upper/lower, upper/upper, lower/upper) that are tested for each stage along with two combinations with one of the fan settings at the upper and the other at an intermediate setting (upper/intermediate, intermediate/upper).

It requires about 15 minutes to achieve steady state conditions for each test point and then the unit is run for an additional 5 minutes at steady state for data collection. With 70 training data points for open lab testing, this would require approximately 24 hours of RTU operation. Therefore, it would be advantageous to significantly reduce the time required for open lab testing. This is accomplished by determining the minimum number of open lab training points required and formulating a set of guidelines for choosing the specific open lab training data points.

The algorithm for selecting the optimal open lab training data points is based on the Fedorov's D-optimal algorithm [17, 18] which is explained as follows and was implemented using Python.

1. Let N be the matrix of candidate points. In this matrix each row represents an experimental run and each column an independent model input variable. In our study, since each compressor stage has 35 open lab testing points and the VRC

sensor has 3 independent input variables (condenser subcooling, evaporator superheat and inlet evaporator quality), this matrix of candidate points is a (35 x 3) matrix.

2. Start with a randomly chosen n-point design matrix X (n x p) from the matrix of candidate points N (35 for this study) where p is the number of independent input variables (also termed predictor variables) in the model, which is 3 for this study. For the first run, n is set equal to p.

3. Compute M , M^{-1} and $|M|$ where $M = X^T X$ is the information matrix. The n rows of the matrix X are n p-dimensional vectors x_i^T , $i = 1...n$. Also note that there are N distinct rows (candidate vectors) x^{jT} from the candidate matrix N.

4. Find simultaneously a vector x_i among n vectors of the current n-point design matrix X and a vector x^j among the N candidate vectors such that the Fedorov's delta function $\Delta(x_i^T, x^{jT})$ is maximum. Exchange x_i with x^j and the new information matrix is related to the previous one by,

$$M_0 = M_1 - (x_i * x_i^T) + (x^j * x^{jT}) \tag{4.1}$$

The corresponding determinants of the information matrices are linked by the relation

$$|M_1| = |M_0| * (1 + \Delta(x_i, x^j)) \tag{4.2}$$

where

$$\Delta(x_i, x^j) = d(x^j) - [d(x_i)d(x^j) - d^2(x_i, x^j)] - d(x_i)$$
$$d(x_i) = x_i^T (M_0)^{-1} x_i$$
$$d(x_i, x^j) = x_i^T (M_0) x^j$$

5. Repeat step 4 until the Fedorov delta function $\Delta(x_i, x^j)$ is less than zero (negative) for all possible couples of (x_i, x^j). The resulting n-point design matrix X is the D-optimal design for the n-point design matrices.
6. Repeat step 2 to step 5 now with n+i- point design matrices X where i=1…N-n and at each run compute the determinant of the information matrix M corresponding to the D-optimal design.
7. Set a threshold on the maximum value of the determinant of the information matrices and choose the optimal experimental data points corresponding to that threshold value. In this study a threshold value of 90% of the maximum value of the determinant of the information matrix is chosen for both stages of operation. This threshold is justified by the fact that the slope of the trace of the inverse of the information matrix becomes relatively constant after this point as shown in Figure 17 and Figure 18.

The D-optimal design minimizes the volume of the confidence ellipsoid of the parameter estimates of the VRC model. The volume of this ellipsoid is inversely proportional to the square root of the determinant of the information matrix. This implies that the D-optimal design maximizes the determinant of the information matrix M. The D-optimal design criteria was chosen over other optimal designs like A-optimal design because the D-optimal design's relatively simple formula has resulted in the development of computer algorithms for the construction of optimal designs for linear regression models. In addition, a D-optimal design also satisfies the criteria of an A-optimal design which minimizes the average variance of the parameter estimates of the VRC model by reducing the trace of the inverse of the information matrix M as shown in Figure 17 and Figure 18.

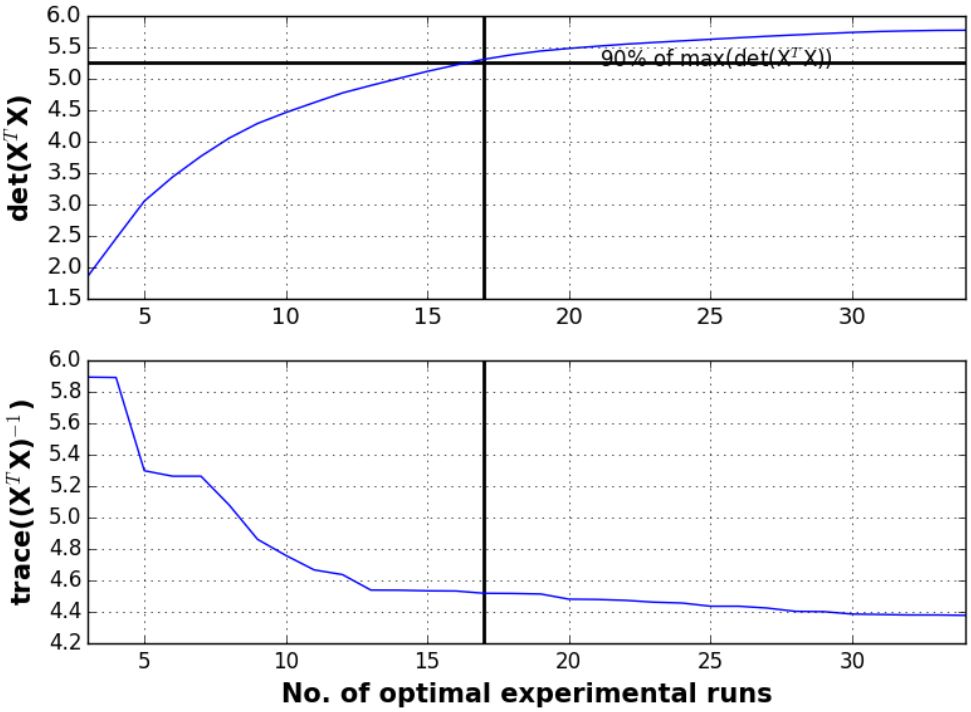

Figure 17. Optimal experimental runs for the first stage of operation.

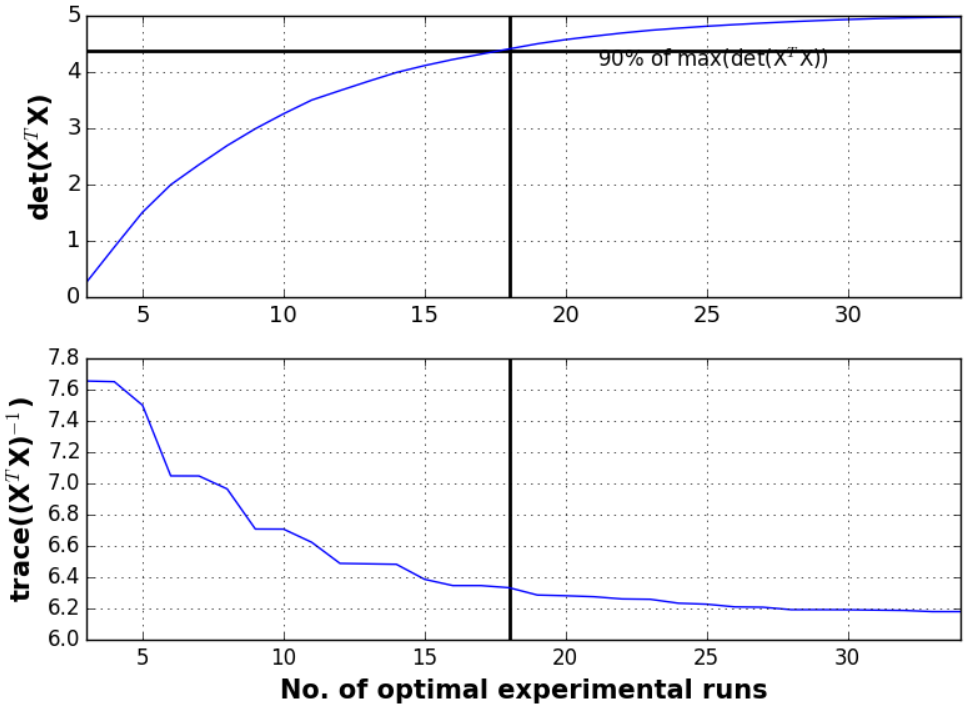

Figure 18. Optimal experimental runs for the second stage of operation.

The number of optimal training points for the first stage of operation is 17 whereas the number of optimal points for the second stage of operation is 18. Therefore, the total number of open lab training points has been reduced to 35 from 70 data points or a 50% reduction in the time required for open lab testing.

4.3 Guidelines for Choosing Operating Conditions for Open Lab Training

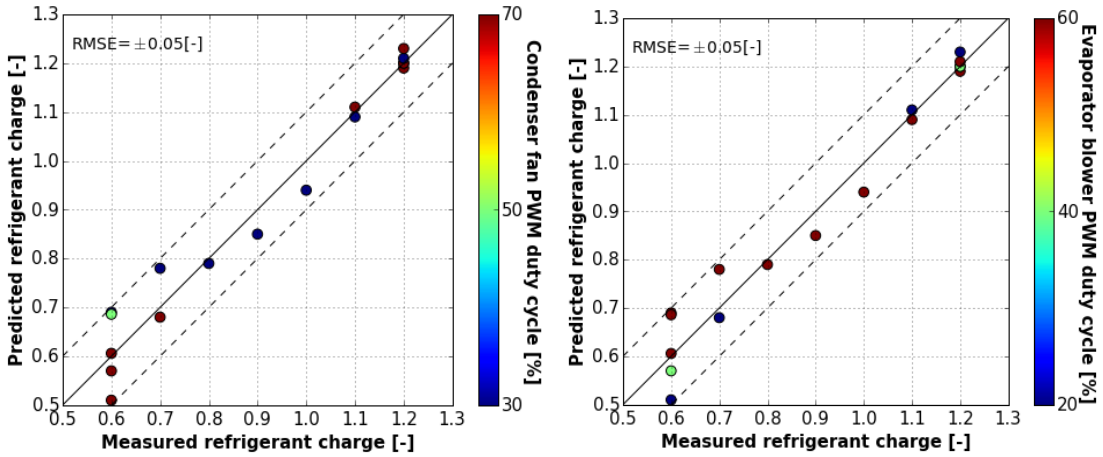

Figure 19. Optimal operating points for open lab training for the first stage of operation (a) condenser fan PWM duty cycle points and (b) evaporator blower PWM duty cycle points.

Table 11. Optimal operating points for open lab training for the first stage of operation.

Charge level [-]	Condenser PWM duty cycle [%]	Evaporator PWM duty cycle [%]
0.6	70	20
0.6	30	60
0.6	70	60
0.6	50	60
0.6	70	40
0.7	70	20
0.7	30	60
0.8	30	60

Table 11. Continued.

0.9	30	60
1	30	60
1.1	30	60
1.1	70	20
1.2	70	60
1.2	50	60
1.2	70	40
1.2	30	60
1.2	70	20

Figure 19 and Table 11 show the optimal test input conditions for charge level and condenser and evaporator fan PWM duty cycles for open lab testing with first stage of compressor operation. These test inputs were determined using the algorithm explained in section 4.2 and include all of the charge levels with diverse combinations of condenser and evaporator fan control inputs that span the range of possible values. A total of 17 test points were chosen from the candidate number of 35 for this study.

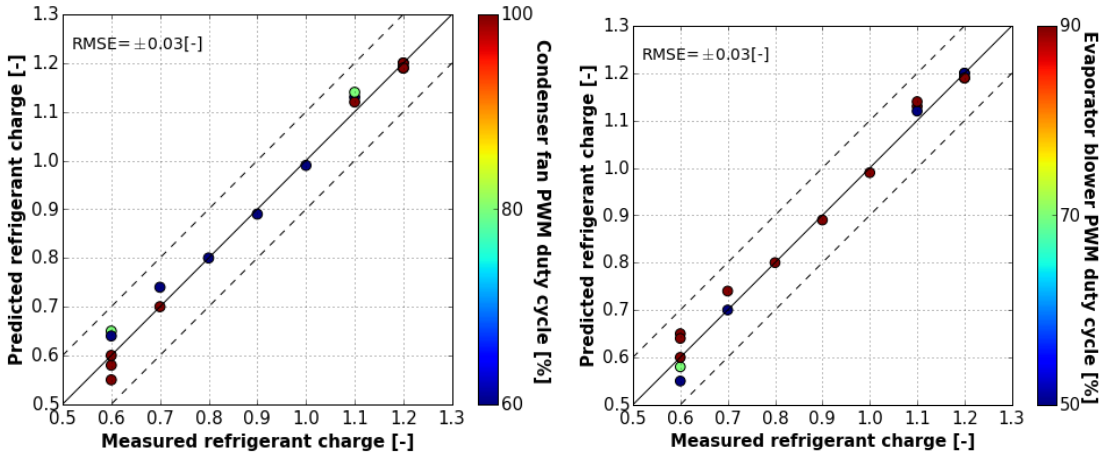

Figure 20. Optimal operating points for open lab training for the second stage of operation (a) condenser fan PWM duty cycle points and (b) evaporator blower PWM duty cycle.

Table 12. Optimal operating points for open lab training for second stage of operation.

Charge level [-]	Condenser PWM duty cycle [%]	Evaporator PWM duty cycle [%]
0.6	100	70
0.6	80	90
0.6	100	50
0.6	100	90
0.6	60	90
0.7	100	50
0.7	60	90
0.8	60	90
0.9	60	90
1	60	90
1.1	60	90

Table 12. Continued.

1.1	100	50
1.1	80	90
1.2	80	90
1.2	60	90
1.2	100	70
1.2	100	50
1.2	100	90

Figure 20 and Table 12 show the optimal open lab test conditions in second stage operation for model training in terms of charge level and condenser and evaporator fan PWM duty cycles. The results are similar to those for first stage with a total 18 operating points out of the candidate set of 35.

Though these operating conditions were chosen a-posteriori based on applying the algorithms in section 4.2 to experimental data, some heuristic guidelines can be formulated for open lab testing based on these results. These guidelines are useful in generalizing the results of this study so that near-optimal test input conditions could be identified for training a VRC sensor for other models of RTU using open lab testing. These can be applied for reducing the time taken for open lab testing for training of the VRC sensor. The guidelines for choosing open lab test inputs for each compressor stage of operations are described as follows:

1. Vary the refrigerant change over the entire range of interest (e.g, 60% to 120% of nominal charge in this study) in increments of 10%. This guideline is derived

directly from the results of Table 11 and Table 12 where all of the refrigerant charge levels were included in the optimal set of training data.

2. At the extreme ends of the charge level domain 60% and 120% of nominal charge level in this study), the condenser and evaporator fan controls should be modulated to include the three out of the four combinations of upper and lower fan settings to be considered for each stage (upper/lower, upper/upper, lower/upper) along with two combinations with one of the fan settings at the upper value and the other at an intermediate setting (upper/intermediate, intermediate/upper).
3. At charge levels other than those at the upper and lower bounds, only employ two combinations of the upper and lower fan settings that are employed for each stage (upper/lower and lower/upper) with no intermediate fan settings. These approximately represent the optimal results of Table 11 and Table 12.

4.4 Validation of the Open Lab Training Methodology

In order to assess the limitations of training a VRC sensor model using open laboratory data, prediction results are compared with those obtained when the model was trained with all of the available data over the entire range of conditions considered. This comparison provides a measure of how well the open lab training data represents the entire range of operating conditions of a typical rooftop unit.

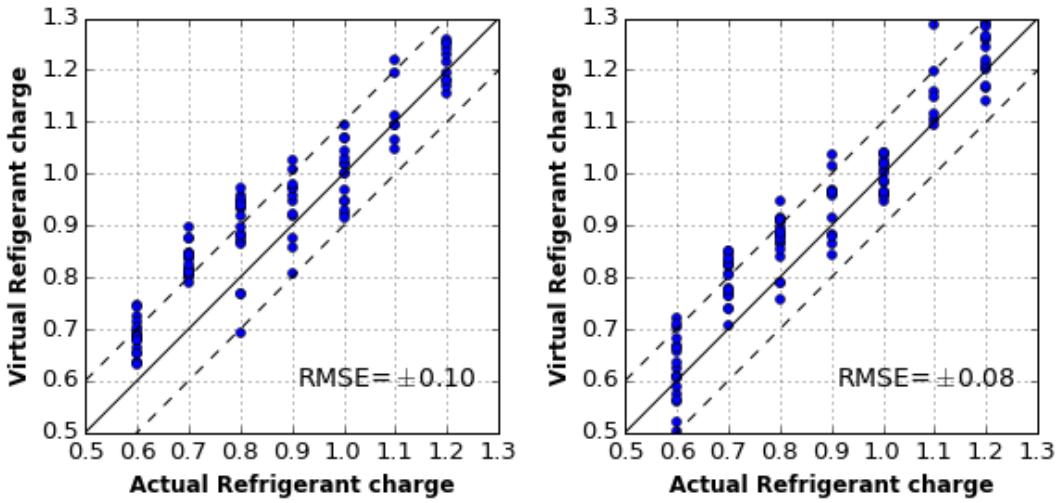

Figure 21. Validation of open lab training methodology for the VRC sensor for the first stage of operation (a) VRC sensor when trained using all open lab training data and validated for all psychrometric room data (b) VRC sensor when trained using all psychrometric room data.

Figure 21 shows how well the open lab training methodology works for the VRC sensor model III for the first stage of operation when trained using all of the open lab training data (35 data points) shown in Table C.1. The comparisons are performed using all of the data (216 points) obtained within the psychrometric chambers. The accuracy of the model in predicting charge level is somewhat worse than the model trained using all of 216 available data points. However, the lower accuracy primarily occurs at low charge levels. The errors close to the nominal charge are less than 10% such that a fault detection algorithm should generally be able to flag charge faults that are outside of this 10% range. The impact of charge on performance is relatively small within 10% of nominal charge so that this is sufficient accuracy for a virtual refrigerant charge sensor.

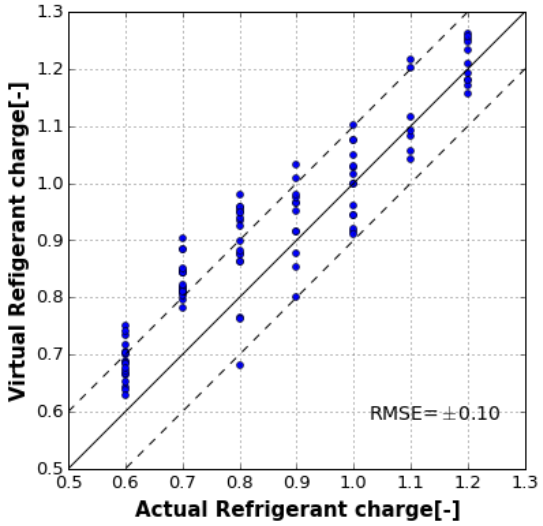

Figure 22. VRC sensor prediction accuracy for first stage of operation when trained using optimal open lab training points in Table 11 but tested over all psychrometric data.

Figure 22 shows the performance of the VRC sensor for first stage when trained with the 17 optimal open lab training data points shown in Table 11. Comparing Figure 21(a) and Figure 22, it can be seen that the optimal data points represent the overall open lab training data points very well. The performance of the VRC sensor has not changed significantly even though the number of training data points has been reduced by 50%.

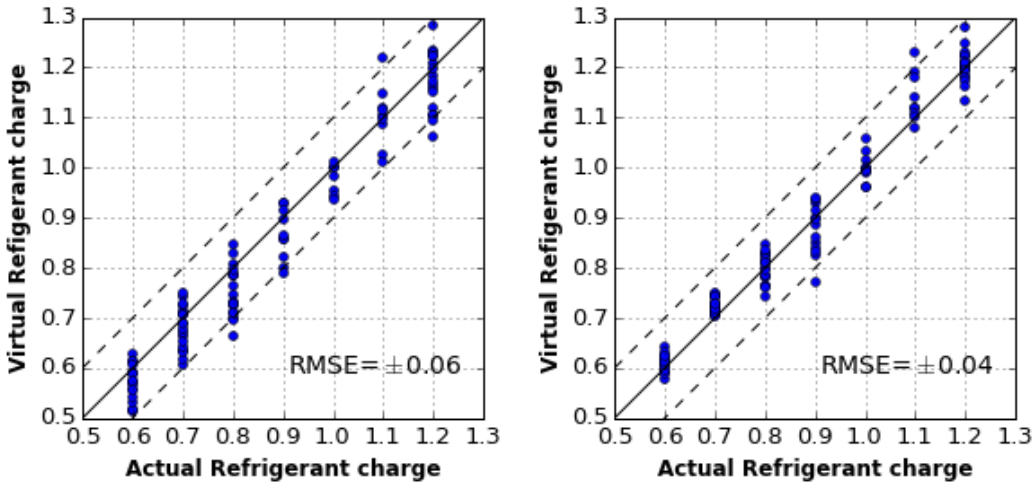

Figure 23. Validation of open lab training methodology for the VRC sensor for the second stage of operation (a) VRC sensor when trained using all open lab training data

and validated for all psychrometric room data (b) VRC sensor when trained using all psychrometric room data.

Figure 23 shows how well the open lab training methodology works for the VRC sensor for the second stage of operation. The errors in charge prediction for training with the 35 open lab training points in Table C.2. are only slightly larger than those associated with training using the 215 data points obtained within the psychrometric rooms at a wide range of conditions. The overall accuracy of the model for second stage operation is quite good with almost all of the predicted charge values within ±10% bounds of the actual charge level.

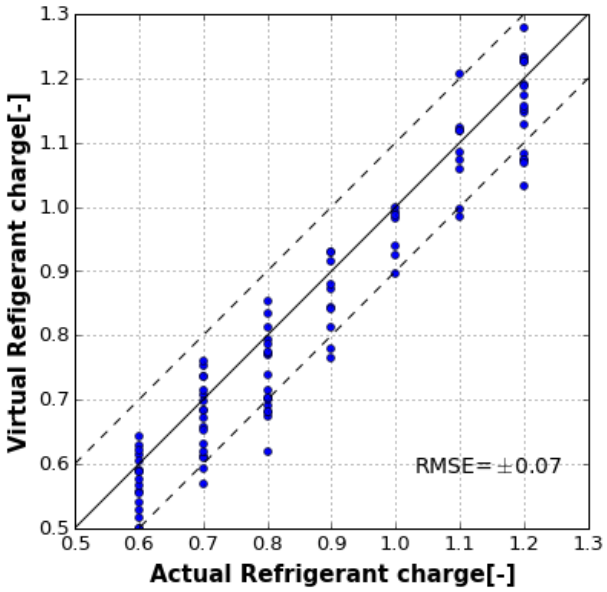

Figure 24. VRC sensor prediction accuracy for second stage operation when trained using optimal open lab training points in Table 12 but tested over all psychrometric data.

Figure 24 shows the performance of the VRC sensor when trained with only the 18 optimal open lab training data points shown in Table 12. Comparing Figure 23(a) and Figure 24, it can be seen that the performance of the VRC sensor has not changed significantly even

though the number of training data points has been reduced by almost 50%. Overall, the optimal training data points represent the overall open lab training data points well.

CHAPTER 5. SUMMARY AND RECOMMENDATIONS

5.1 Summary

The study presented here extended virtual sensors for measuring refrigerant charge, compressor power and refrigerant mass flow rate to rooftop units having micro-channel condensers. In addition, a methodology to minimize the training requirements for virtual refrigerant charge sensors was developed that significantly reduces the training costs and time associated with implementing virtual charge sensors for new equipment.

Analysis of virtual refrigerant charge sensor results showed that accuracy is improved when including inlet evaporator quality as an input variable along with condenser subcooling and either evaporator superheat or compressor discharge superheat. The use of three independent input variables decreased the bias and RMSE for model predictions of refrigerant charge compared to the original model form that only employed two input variables. Overall, the performance of the virtual charge sensor was good with most of the charge predictions within ±10% of the actual refrigerant charge.

The virtual compressor power sensor, which is based on the AHRI compressor map, worked very well for both stages of operation over the entire range of operating conditions tested. The virtual cooling capacity sensor, which is based on a virtual

refrigerant mass flow rate sensor determined with the AHRI map, also was shown to work very well for conditions where reliable direct mass flow measurements weravailable.

However, only limited direction measurements were available for second stage operation because of saturation of the micro-motion mass flow meter. The results for first stage and limited second stage test points were excellent.

Cost estimates for implementation of the virtual sensors within an embedded system were performed and compared with cost estimates associated with using direct measurements. It was shown that the cost of virtual sensor implementation would be in the range of $60 - $100 per unit, depending on whether the algorithm could be deployed within the existing controller or an additional microprocessor were necessary. In contrast, the cost of implementing a monitoring system with direct measurements of only compressor power consumption and cooling capacity would be about $700 per unit and doesn't include a refrigerant charge sensor. There is not a practical way of directly measuring the amount of refrigerant charge while the unit is in operation.

The methodology that was developed for minimizing the training costs and time for the virtual refrigerant charge sensor involves running the unit in an open lab space instead of the psychrometric chambers. In addition, an algorithm was implemented to determine the minimum number of open lab training points required and the results of this analysis were used to establish a set of guidelines for specifying near-optimal input conditions for running the open lab testing. An evaluation of the open lab training methodology was carried out and it was shown to provide virtual sensor performance similar to that obtained using all of the data from psychrometric room test data for training.

The virtual sensors could be implemented in a micro-controller and could be made as an embedded part of the rooftop unit. Furthermore, the open lab training methodology could be entirely automated and implemented as a training kit with necessary hardware, sensors

and software to modulate the amount of refrigerant charge, condenser and evaporator air flow rate and collect the required data to train the virtual charge sensor. This training kit based on open lab testing could significantly speed up the process and reduce the cost of acquiring the calibration data for virtual charge sensors and thus could improve the overall economics of applying virtual sensors for a whole RTU product line.

5.2 Recommendations for Future Work

Future work could include a direct evaluation of how the accuracy of the virtual charge sensor is influenced by the type of condenser, since the condenser is one of the primary locations for refrigerant mass. This goal could be accomplished by replacing the existing micro-channel condenser of the case study RTU with a conventional round-tube, finned condenser and then repeating the virtual charge sensor evaluation. In addition, it would be useful to evaluate virtual charge sensors for units having micro-channel heat exchangers for both the evaporator and condenser.

LIST OF REFERENCES

LIST OF REFERENCES

[1] H. Li and J. Braun, "Decoupling Features and Virtual Sensors for Diagnosis of Faults in Vapor Compression Air Conditioners," *International Journal of Refrigeration,* vol. 30, no. 3, pp. 546-564, 2007.

[2] H. Li and J. Braun, "“Development, Evaluation, and Demonstration of a Virtual Refrigerant Charge Sensor," *HVAC&R Research,* vol. 15(1), pp. 117-136, 2009.

[3] W. Kim and J. Braun, *Fault Detection And Diagnosis For Air Conditioners And Heat Pumps Based On Virtual Sensors,* West Lafayette, IN: Purdue University, 2013.

[4] W. Kim and J. Braun, "Virtual Refrigerant Mass Flow and Power Sensors for Variable-Speed Compressors," in *International Refrigeration and Air Conditioning Conference*, West Lafayette, IN, 2012.

[5] CEC, "California Energy Commission," 2013. [Online]. Available: http://www.energy.ca.gov/title24/.

[6] CEC, "California Energy Commission," 2016. [Online]. Available: http://www.energy.ca.gov/title24/2016standards/index.html.

[7] A. Cowan, "Review of recent commercial roof top unit field studies in the Pacific Northwest and California," Portland, Oregon, 2004.

[8] J. Proctor and T. Downey, "Heat Pump and Air conditioner Performance," in *Affordable Comfort Conference*, Pittsburgh, PA., 1995.

[9] H. Li and J. Braun, "Apparatus and method for determining refrigerant charge level," U.S. Patent Application serial number 11/624,377., 2006.

[10] I. H. Bell, J. Wronski, S. Quoilin and V. Lemort, "Pure and Pseudo-pure Fluid Thermophysical Property Evaluation and the Open-Source Thermophysical Property Library CoolProp," *Industrial and Engineering Chemistry Research,* vol. 53, no. 6, pp. 2498-2508, 2014.

[11] H. Li and J. Braun, "Development, Evaluation and Demonstration of a virtual refrigerant charge sensor," *HVAC&R Research,* vol. 15, no. 1, pp. 117-136, 2009.

[12] W. Kim and J. Braun, "Fault detection and diagnosis for air conditioners and heat pumps based on virtual sensors," West Lafayette, 2013.

[13] W. Kim and J. Braun, "Virtual Refrigerant Mass Flow and Power sensors for variable speed compressors," in *International Refrigeration and Air conditioning conference*, West Lafayette, 2012.

[14] Rice. C and A. E. Dabiri, "A compressor simulation model with corrections for the level of suction gas superheat," in *ASHRAE transactions*, 1981.

[15] TIAX, "Energy impact of commerical building controls and performance diagnostics," 2005.

[16] "Omega online catalog," [Online]. Available: http://sea.omega.com/sg/pptst.

[17] V. Fedorov, Theory of optimal experiments, New York: Academic Press, 1972.

[18] P. Aguiar, B. Bourguignon, M. Khots and D. Massart, "D-optimal designs," *Chemometrics and intelligent laboratory systems,* vol. 30, pp. 199-210, 1995.

APPENDICES

Appendix A. Experimental Data From Psychrometric Chambers

Table A.1.

Data for the first stage of compressor operation comprising of air temperatures, refrigerant mass flow rate and compressor input power.

Test	$T_{in,air,cond}$	$T_{out,air,cond}$	m_{ref}	W_{comp}
[-]	[°C]	[°C]	[g/s]	[W]
0	22.43394241	25.49263525	36.32654	1785.19
1	22.79553145	25.80611714	34.65998	1789.205
2	22.21122946	25.382644	39.70964	1802.751
3	21.82822128	26.1058156	31.99426	1830.331
4	21.80091429	30.91178231	51.91887	2086.725
5	21.83865672	26.39328358	32.47617	1827.915
6	29.46528182	34.24419697	62.86456	2280.578
7	29.40466005	38.46052936	69.91184	2555.181
8	30.1706215	33.36165109	64.82031	2230.897
9	29.43312736	34.21767296	62.35271	2266.739
10	30.15382809	33.6572956	65.58174	2241.71
11	30.20792771	33.76819277	65.95397	2236.479
12	30.43991816	35.01087809	72.21886	2712.824
13	30.45565803	40.5382038	73.53286	3078.299
14	30.43332011	34.84375826	71.35874	2709.956
15	30.82344754	35.0503212	70.46739	2675.715
16	31.03397556	35.35021045	72.15642	2688.205
17	31.01965125	35.47228944	72.88418	2682.493
18	36.50295749	41.21847875	64.92204	2239.78
19	36.58531178	45.69987683	62.48562	2308.609
20	36.4875702	40.98928367	70.43046	2601.25
21	35.54646964	39.88935223	61.42157	2275.597
22	36.95583404	40.46387943	65.14756	2240.376
23	37.11963065	40.58673215	64.77249	2247.086
24	36.59945098	41.43098856	87.37117	3739.817
25	36.49617993	46.54254902	81.98407	3325.44
26	36.572216	41.22848	81.04918	3384.896
27	37.29132237	41.64458882	78.2287	3405.485
28	37.37905367	41.97056026	34.45416	1819.539
29	36.68399174	41.91235537	49.42304	2083.915
30	43.67526606	48.00766055	40.70334	1805.708
31	43.63700234	53.21437939	35.0145	1796.784

Table A.1. Continued.

32	43.91644097	49.28727431	34.58022	1795.86
33	43.93794828	47.93751232	36.90188	1794.639
34	44.18440797	48.23767236	72.10793	2738.812
35	43.80634453	48.32081618	74.51495	3076.661
36	30.43244344	33.25386124	72.28311	2741.698
37	29.4872449	34.82414966	72.16177	2673.28
38	29.4182801	39.18769861	73.38778	2698.632
39	29.40503812	34.73880743	73.95893	2703.897
40	29.90655138	33.64509607	69.12954	2698.046
41	30.44087526	33.86985685	70.45228	2697.845
42	30.45324031	41.35102067	67.41281	2742.243
43	30.52733333	35.66628019	70.48898	3298.016
44	31.53541104	35.8197137	67.83358	2802.51
45	30.59604934	35.58340923	69.74901	2712.005
46	21.77783673	26.38339002	68.23432	2686.648
47	21.59034615	30.87415501	65.48475	2245.909
48	21.73075177	26.42908983	58.38487	2324.983
49	22.68452109	25.33991729	59.30414	2302.755
50	22.93641566	25.78917671	61.6798	2237.332
51	22.89698165	25.99227829	60.8382	2234.44
52	36.41256734	41.3848042	41.72439	1844.09
53	36.4794716	46.0337037	54.46489	2155.765
54	36.43738053	41.69991888	50.17522	1846.596
55	37.283385	40.05343333	33.91261	1807.984
56	37.3797622	40.44757114	38.29058	1785.14
57	37.44565957	40.68092199	45.4397	1783.255
58	36.8634569	42.97109914	61.16078	2702.794
59	36.54464894	48.00352837	55.41272	2262.587
60	36.74648988	42.58595142	57.46521	2408.699
61	37.24258431	41.92911765	57.77205	2264.986
62	37.88138617	42.40450815	51.05132	2259.333
63	38.17851966	42.56797151	64.94363	3217.439
64	30.61682008	35.89	62.43232	2828.883
65	30.8082	35.10059184	61.1804	2730.916
66	43.7523466	49.05277127	61.29863	2741.308
67	43.66907669	54.97283231	62.95802	2744.478
68	44.1118843	50.65444628	36.22437	1804.565
69	41.94343628	48.48306347	54.52613	2149.973
70	43.49607449	49.02729872	53.29781	1851.993

Table A.1. Continued.

70	43.49607449	49.02729872	53.29781	1851.993
71	44.47057908	49.3213417	47.4152	1798.853
72	36.84262913	40.2340712	54.79651	1801.378
73	36.58279607	40.59785422	50.71437	2303.202
74	36.47782215	41.66810192	59.87818	2309.828
75	36.84004762	47.97271825	55.8526	2432.494
76	36.55822503	42.34702065	61.71323	2737.263
77	35.17693555	40.69516286	59.16574	2370.049
78	29.52608416	40.29040429	70.77434	2319.15
79	29.87552174	33.64078502	57.36894	2770.972
80	29.46980344	35.09931204	71.06417	2769.226
81	29.3898895	35.12383978	77.83772	2770.71
82	30.40052807	33.72399168	51.83853	1854.959
83	30.09389648	33.92722567	57.57059	2202.493
84	21.80743729	27.05893785	57.10646	1857.714
85	21.80816949	32.51926554	49.43364	1835.269
86	21.82140909	27.4534596	60.92188	1835.458
87	21.26581301	25.52819783	73.02037	1824.506
88	22.64479191	25.76988439	71.74113	2798.308
89	22.7324573	26.03067952	77.29598	2787.883
90	31.06339535	35.10192389	80.19139	2794.887
91	30.42492212	42.07101765	62.90185	2331.473
92	30.54575263	35.83979825	75.36356	2302.805
93	31.26847415	35.60562686	78.87014	2308.664
94	30.55164792	35.63528932	54.18844	1832.17
95	31.29994937	35.85438819	74.84331	1821.738
96	36.89279116	42.95505355	77.39009	1831.213
97	36.52305747	47.85795402	73.61101	2758.175
98	36.72421557	42.5476181	77.45019	2882.742
99	38.43507021	42.18671727	77.60694	2964.704
100	38.13714188	42.42703134	78.07833	3606.178
101	38.21391111	42.68410826	79.08085	3027.768
102	43.95230099	49.89755116	79.24416	2762.033
103	43.58763291	54.93651195	72.79821	2360.299
104	43.80209368	49.70577674	77.41099	2448.652
105	44.6891547	49.07812615	77.22734	2357.866
106	44.88376873	49.44559975	79.44547	2904.287
107	44.71103098	49.68386021	79.47655	2473.051
108	29.47882178	40.31554455	79.78933	2369.849

Table A.1. Continued.

109	30.15361995	34.02600158	71.79251	1889.206
110	29.74994138	36.38414943	76.54537	1840.616
111	29.64349145	34.2051567	76.3523	1906.039
112	30.05484281	33.80429208	79.84697	2271.727
113	36.50610384	47.1520015	79.16944	1818.599
114	36.52279913	42.44729985	79.04282	1926.147

Table A.2.

Data for the first stage of compressor operation comprising of refrigerant temperatures.

Test	$T_{out,ref,evap}$	$T_{out,ref,comp}$	$T_{out,ref,cond}$	$T_{sat,evap}$
[-]	[°C]	[°C]	[°C]	[°C]
0	24.61921466	59.72243455	25.79633508	7.608664921
1	25.05672451	59.25481562	26.10852495	8.43791757
2	23.79569405	59.838017	25.72167139	6.662691218
3	24.6072766	60.03442553	26.76995745	8.259702128
4	25.00265306	64.08293878	31.22865306	10.14436735
5	24.94522388	59.56421642	26.97955224	8.925149254
6	25.47336364	68.74011364	34.52477273	10.50581818
7	25.71977667	72.73545906	38.49094293	12.29811414
8	24.60018692	68.92436916	33.33205607	8.979742991
9	25.75033019	68.0592217	34.48556604	11.08462264
10	25.42654088	68.64926625	33.64092243	10.03150943
11	25.76679518	68.09491566	33.84154217	10.56648193
12	26.38076063	76.54548098	41.35742729	13.06120805
13	26.49810624	82.16660508	45.53595843	13.92612009
14	26.0274212	76.95830946	41.08604585	12.47805158
15	25.44607287	76.52635628	39.64226721	11.07593117
16	26.14714894	76.78734043	40.17431915	12.01468085
17	26.24679764	76.24717092	40.36119843	12.41119843
18	23.470181	66.50735294	33.47074661	9.991312217
19	24.89119898	67.035	35.01239796	11.54114796
20	25.1429484	71.47675676	39.24825553	13.20764128
21	25.10407625	66.33369501	34.99296188	12.08554252
22	24.67586466	66.28130326	33.72834586	11.13626566
23	25.06196319	65.84746421	34.13257669	11.89832311
24	25.07503876	78.79678295	41.64717054	11.46833333
25	25.02855072	72.99402899	36.30446377	10.20005797

Table A.2. Continued.

26	25.08629857	73.53206544	36.29977505	10.35912065
27	24.74910816	73.85047438	35.93231499	9.603870968
28	24.22268707	57.68792517	26.98363946	9.563571429
29	24.65314685	61.19337413	31.07751748	11.57267483
30	24.66620567	56.80964539	26.9864539	10.38847518
31	22.94722084	57.69754342	25.93059553	7.989851117
32	24.11918675	57.62051205	26.3663253	9.434126506
33	24.58490826	57.02323394	26.57779817	10.22830275
34	25.01234957	75.37412607	41.45123209	13.05318052
35	25.74977778	80.52419753	45.92691358	14.73479012
36	25.68849558	75.05902655	41.7494469	13.75584071
37	24.024425	74.6613	40.11545	12.091325
38	25.05704268	74.65634146	40.44640244	12.9977439
39	25.59804965	74.27170213	40.71758865	13.63592199
40	23.04141748	73.42765049	40.28732039	12.11765049
41	24.57594595	73.5344226	40.58039312	13.27938575
42	25.17480499	76.10911076	41.82405616	12.97332293
43	25.97306548	84.38916667	47.99547619	14.38372024
44	25.85042984	76.41480405	42.5211378	13.65831858
45	25.14428274	72.93906445	40.59293139	13.72471933
46	24.98668317	72.04158416	40.15487624	13.71064356
47	22.39985507	64.24014493	33.63601449	10.88351449
48	23.88164619	66.05810811	35.25339066	11.61152334
49	24.64433702	65.46450276	35.3509116	12.47149171
50	23.90068607	64.55767152	33.86116424	11.90345114
51	24.46975155	64.14349896	34.13981366	12.46248447
52	23.78589831	57.01762712	27.52037288	10.24128814
53	24.26508475	61.87661017	32.61101695	12.13325424
54	24.39723485	56.54818182	27.85424242	11.15719697
55	22.08247967	55.35373984	25.90487805	8.868373984
56	23.76222543	55.88586705	26.30803468	10.24511561
57	24.35245179	55.44413223	26.59016529	11.11889807
58	24.50012376	72.22725248	40.44378713	13.19376238
59	23.27890736	64.22213777	34.21947743	11.9656057
60	24.56493103	67.01605172	36.58463793	12.48213793
61	24.08128205	63.73760684	34.45544872	12.74352564
62	21.50464883	63.69648829	33.9348495	10.87050167
63	24.83819413	82.35419865	47.28241535	14.12487585
64	24.81141921	75.83585153	42.66971616	13.38340611

Table A.2. Continued.

65	21.37078189	72.331893	40.54794239	11.91314815
66	23.18079332	73.14638831	41.07392484	12.94580376
67	24.17343348	72.86184549	41.37914163	13.85339056
68	21.30221402	54.26380074	26.26693727	9.415940959
69	24.20848837	61.75639535	32.47549419	12.1302907
70	24.28689873	56.46528481	27.9125	11.21917722
71	22.86374603	54.81653968	26.476	10.4972381
72	23.67840849	54.60403183	26.84267905	11.52023873
73	20.28982587	63.73447761	34.11696517	10.06756219
74	22.309375	64.07805556	34.64835648	11.67217593
75	22.57108527	66.36418605	36.46100775	11.61271318
76	23.39818182	71.6244289	40.80578089	13.14037296
77	23.68818182	65.33703896	36.10163636	12.46145455
78	23.42550218	63.74646288	34.87334061	12.64617904
79	20.45543767	72.60241379	40.87774536	11.27549072
80	22.59285408	73.0316309	41.26802575	12.67420601
81	23.83567816	72.75832184	41.07708046	13.52917241
82	22.39573134	55.52373134	27.54173134	10.29202985
83	23.07089595	61.04881503	32.93179191	12.23375723
84	23.25145205	55.11030137	27.82649315	11.32687671
85	20.32613636	54.11212121	26.38886364	8.955505051
86	22.17813747	54.39789357	26.82181818	10.60611973
87	23.13851385	54.07511335	27.0002267	11.73380353
88	18.63882206	71.37258145	40.95323308	11.25451128
89	21.03569647	71.62777547	41.15806653	12.93243243
90	22.85283447	71.83875283	40.44598639	13.91825397
91	17.46157233	60.97814465	34.13858491	10.06849057
92	21.16682573	62.79454357	34.27877593	11.76342324
93	22.43200855	62.60474359	33.25457265	12.64632479
94	18.49960289	51.893213	26.3599639	9.213429603
95	20.94167102	53.13770235	26.19877285	10.8902611
96	22.00797654	53.25577713	25.10002933	11.69832845
97	17.67752809	69.6058427	38.07525843	10.89739326
98	20.47922078	72.27928571	37.85272727	12.54655844
99	20.02241007	73.76107914	39.51352518	12.72291367
100	22.11634409	85.09724731	41.4228172	13.9372043
101	21.94391685	74.57564551	38.26407002	13.49925602
102	22.03261702	70.97580851	36.20359574	13.33097872
103	16.13369186	60.60639535	30.99488372	9.738023256
104	19.874875	63.707425	33.2523	11.889275

Table A.2. Continued.

105	19.87580838	61.98457086	32.1396008	11.78694611
106	21.77977578	72.23246637	35.61121076	13.38257848
107	21.70792952	64.6088326	32.35209251	12.9035022
108	21.6860479	62.26313373	31.28984032	12.84870259
109	15.54623853	50.33189602	25.69266055	8.896911315
110	19.47667656	50.41005935	25.00014837	11.0579822
111	19.67437318	52.37052478	26.5135277	11.07104956
112	20.24813953	58.56860465	30.45965116	12.69372093
113	21.05991736	50.99280992	24.49177686	11.99367769
114	21.1957732	53.17810997	25.66171821	12.09388316

Table A.3.

Data for the first stage of compressor operation comprising of refrigerant pressures.

Test	$P_{in,ref,comp}$	$P_{out,ref,comp}$	$P_{out,ref,cond}$
[-]	[kPa]	[kPa]	[kPa]
0	982.8123141	1780.631984	1698.783398
1	1001.243247	1793.352527	1709.782985
2	956.8721048	1781.270861	1701.668289
3	991.1056851	1818.199996	1733.175749
4	1041.436865	2053.788273	1963.19202
5	1013.312728	1839.449575	1752.796649
6	1053.480602	2215.766445	2122.618007
7	1098.607052	2459.343313	2361.355385
8	1013.175638	2153.398217	2063.961294
9	1068.463068	2215.503811	2122.213455
10	1040.763495	2172.109352	2080.671057
11	1063.231373	2184.111595	2092.812147
12	1117.057875	2602.594038	2503.114987
13	1146.692169	2893.245102	2794.961843
14	1104.333762	2586.063223	2488.37255
15	1075.637223	2532.315316	2433.610526
16	1097.317853	2552.805213	2455.574168
17	1108.708365	2560.320088	2463.671212
18	1037.950339	2168.793774	2080.232412
19	1091.226179	2252.292298	2162.966684
20	1138.109354	2519.016698	2426.868555
21	1107.156988	2249.870305	2161.535026

Table A.3. Continued.

22	1089.230484	2203.11201	2109.95989
23	1102.611519	2212.484851	2121.19038
24	1044.439624	2683.414806	2577.270663
25	1015.12422	2348.373041	2243.9056
26	1017.879562	2358.534949	2249.788838
27	995.501962	2344.178907	2235.532567
28	1040.205864	1843.163956	1763.365752
29	1083.754386	2053.856566	1968.905598
30	1063.62623	1846.245777	1765.401277
31	992.3962233	1795.033891	1713.474816
32	1036.363142	1822.267461	1737.679774
33	1060.515225	1833.305273	1749.132362
34	1131.571696	2622.249014	2529.629415
35	1179.570578	2930.302316	2838.757279
36	1152.13944	2644.255657	2552.321403
37	1091.047195	2542.819365	2446.12086
38	1121.108241	2569.83671	2472.71846
39	1149.104014	2589.838465	2494.152323
40	1102.125317	2567.178159	2472.461289
41	1143.937192	2595.861393	2498.527926
42	1126.139384	2639.756226	2551.381017
43	1175.898542	3075.862926	2994.673208
44	1150.536603	2682.973802	2595.488383
45	1170.242058	2615.108501	2518.618272
46	1152.840183	2579.96748	2492.538812
47	1068.620268	2185.777888	2094.020511
48	1102.259985	2273.003504	2184.195658
49	1129.380307	2281.116072	2194.133641
50	1102.006888	2206.118913	2112.8008
51	1130.022197	2228.09617	2134.992164
52	1068.007654	1878.915976	1795.292539
53	1120.214698	2153.446298	2066.709322
54	1096.596958	1897.781659	1813.381242
55	1024.702199	1802.892455	1718.075215
56	1063.271168	1828.927561	1742.093795
57	1090.31408	1843.091804	1755.704251
58	1147.085186	2594.530116	2513.021275
59	1116.9482	2240.009919	2148.41415
60	1132.315395	2351.745445	2270.098203

Table A.3. Continued.

61	1143.489073	2253.941199	2163.492043
62	1073.25496	2204.850465	2120.826301
63	1175.659422	3029.429542	2954.486655
64	1151.077223	2703.011127	2625.835155
65	1101.617243	2590.835436	2502.565216
66	1136.16918	2623.116163	2538.077438
67	1165.674562	2642.05973	2556.058455
68	1037.151266	1815.133317	1733.009162
69	1116.370567	2145.93091	2063.332044
70	1097.645991	1903.561291	1821.512244
71	1078.586429	1847.349016	1756.917438
72	1108.876891	1866.134851	1775.835446
73	1057.910107	2224.696371	2143.531179
74	1110.302269	2262.762833	2179.328831
75	1109.17614	2353.092147	2273.234341
76	1153.66252	2630.136538	2552.08703
77	1138.182029	2332.890047	2252.197678
78	1145.554358	2284.437417	2201.134384
79	1092.057966	2613.489424	2538.067233
80	1137.310541	2643.954925	2566.790835
81	1171.064625	2661.322593	2582.694906
82	1074.346409	1889.499839	1808.227821
83	1120.805777	2174.704509	2092.395014
84	1104.121288	1905.362904	1822.680156
85	1028.250316	1836.564159	1754.103144
86	1081.310596	1863.851477	1776.971408
87	1119.135237	1886.377476	1798.285378
88	1093.054459	2636.17194	2564.23509
89	1146.483538	2667.204823	2591.674459
90	1179.675478	2690.910057	2613.145417
91	1054.827541	2231.854884	2162.319991
92	1116.414386	2269.947923	2189.656938
93	1150.458321	2289.275103	2209.11138
94	1033.996011	1831.104715	1756.244238
95	1092.337611	1874.767546	1790.914833
96	1122.84324	1894.078235	1810.03056
97	1088.16422	2616.363715	2552.010843
98	1143.989461	2723.067844	2657.851422
99	1143.63282	2796.764777	2733.748043
100	1185.212056	3315.337619	3259.341763

Table A.3. Continued.

101	1173.483939	2851.245298	2789.245223
102	1168.672464	2665.359798	2602.618017
103	1045.926163	2251.446355	2182.838299
104	1124.757155	2377.434493	2308.070243
105	1118.704527	2301.1002	2230.180036
106	1171.676247	2762.924244	2697.785632
107	1158.464828	2414.235515	2344.78452
108	1156.172375	2332.672046	2261.091723
109	1018.518343	1859.509661	1788.083272
110	1096.911795	1867.95665	1792.810383
111	1103.143493	1929.432548	1849.42679
112	1151.045012	2254.696233	2183.589314
113	1134.771335	1891.530727	1813.98407
114	1140.344134	1978.026962	1897.438052

Table A.4.

Data for the second stage of compressor operation comprising of air temperatures, refrigerant mass flow rate and compressor input power.

Test	$T_{in,air,cond}$	$T_{out,air,cond}$	m_{ref}	W_{comp}
[-]	[°C]	[°C]	[g/s]	[W]
0	36.91311523	40.47872428	72.21923095	3259.707018
1	37.06919833	40.87477383	82.33412642	3646.685254
2	37.21170815	41.15905579	70.30445354	3271.730909
3	22.8157048	25.77856089	70.25650343	3278.188944
4	21.73973256	32.23625	72.87113727	3316.717501
5	21.88638608	27.48540084	74.17480605	3346.421744
6	22.2504127	26.03077249	84.08584902	3729.763311
7	22.66017507	26.31201592	91.72954256	4181.303003
8	36.5025614	48.05046784	83.5066996	3728.75536
9	36.50048254	42.16621164	83.38874918	3794.889562
10	38.08319933	42.65508654	85.94254732	3854.817768
11	36.13528736	41.97072797	88.19180014	3864.170888
12	38.07939552	42.92146766	87.78883807	4268.984789
13	30.81490802	35.70137639	94.15568946	4777.564258
14	29.44193855	41.02359404	90.86124792	4446.129432
15	29.44781328	34.86638313	90.71450172	4322.641477
16	31.28003475	35.88692407	92.65808354	4341.003659

Table A.4. Continued.

17	31.2338125	36.14245833	93.75607476	4400.313539
18	43.9373361	50.72260489	87.91761552	3854.117353
19	43.91452399	49.24396064	96.36639309	4302.386569
20	42.93189	49.36048333	89.04941397	3789.086905
21	42.87116585	48.96854472	88.44688941	3864.64459
22	30.46429353	33.76751244	90.62597656	3880.868703
23	30.41788426	34.31426698	91.36109726	3883.194246
24	29.80448062	36.35395349	78.46122008	3346.646234
25	29.41795338	40.65104118	73.93597918	3334.40979
26	29.58393766	35.86067532	95.5182808	4349.271368
27	30.09026638	34.55352256	101.7581868	4793.958814
28	36.76180371	40.5183466	98.7622805	4558.139145
29	36.63096137	40.90574392	94.74901409	4456.789112
30	35.97646437	41.02050575	97.32478081	4491.461572
31	21.83434627	27.13845771	99.34498678	4477.182587
32	21.75076879	32.70183044	76.92563087	3324.410829
33	21.80393973	27.45122374	91.55728567	3789.056798
34	22.93021212	25.77228114	89.32963211	3373.958116
35	23.02913525	26.29266075	83.81583458	3373.086929
36	23.06872544	26.63723762	81.48166699	3351.867567
37	31.28553875	35.73389414	89.04581646	3416.254443
38	31.56998795	36.29547523	88.82903353	3877.234478
39	31.73098491	36.64922013	96.81081011	4337.533285
40	36.23365696	41.99981661	91.56120479	3814.786607
41	38.37315572	43.08399625	89.50031765	3816.432063
42	37.9639386	42.73869152	91.48538188	3894.381891
43	44.42420915	50.25030501	94.10122632	3922.602484
44	44.56843004	49.74101129	96.60227505	4479.618568
45	44.41648675	49.56264349	101.6524308	4921.84619
46	36.89380451	40.71944862	98.44292389	4414.388876
47	37.00767152	41.17295911	96.0531279	4389.769959
48	36.85172789	41.37996221	99.43122849	4458.777889
49	29.45222642	33.86901468	101.0750026	4504.668896
50	29.99850622	34.20596127	99.45612667	4239.317498
51	29.44017949	34.40440171	95.08454159	3763.813203
52	22.92305415	25.77086643	94.5690263	3907.115782
53	22.99437598	26.1808007	92.9189046	3847.992853
54	22.82767155	26.44360704	100.4507142	3926.736535
55	37.02671933	42.84786556	86.65688513	3363.5402

Table A.4. Continued.

56	37.7965082	43.02744991	95.36337263	3757.813355
57	36.97304425	42.67544985	98.46082718	3324.794241
58	30.42985409	35.68723013	90.19895309	3396.400133
60	30.96847505	36.31556221	101.8750082	4579.227855
61	43.73782955	49.58030303	101.4515961	4487.217432
62	44.01624484	49.39177974	103.1224247	4520.311343
63	43.84274094	49.21433557	101.6052095	4370.326973
64	36.60070562	39.90493633	94.06404612	3379.957482
65	36.86735065	41.20428571	100.9720496	3457.514127
66	36.50865468	42.76092326	103.0416928	3479.134362
67	36.55497634	47.90639427	100.4332634	3834.724492
68	36.47819694	42.64345004	103.2677189	3941.461201
69	36.52710213	39.73025532	103.2695539	3933.098713
70	29.54405233	33.49637597	102.2164906	4577.689407
71	29.67261	35.92290833	103.2527455	4539.063866
72	30.80550499	34.44286094	103.2555868	4573.234705
73	29.13404933	41.13784006	103.3174358	4041.174418
74	29.62771806	36.03735683	103.2722016	4040.482172
75	30.6997006	34.58896873	102.1263064	3942.233261
76	23.61793272	26.14603466	100.5148203	3409.231692
77	22.8472819	26.077636	102.8010553	3457.524806
78	21.74840233	27.59025267	103.2880834	3518.788267
79	21.41516279	33.42155039	103.1396449	4644.495225
80	22.60905785	26.3892011	103.2421701	4695.953836
81	21.81235052	28.23155785	103.2532776	4702.671862
82	36.34943602	41.02240126	101.2390668	4091.325848
83	36.56601143	40.15961905	103.3481406	3986.521194
84	36.5375666	41.44601723	103.2616372	4061.429435
85	36.60466465	48.7227996	103.2604733	4953.184758
86	36.52643492	40.44821164	103.2891841	4002.026173
87	36.83242254	43.08139906	103.2294254	4330.980014
88	30.62259914	43.78545977	103.2515828	4296.720584
89	30.43279638	34.69816742	99.61193597	3534.925163
90	31.31550746	36.9480908	103.3258937	3647.100373
91	31.75222914	35.95448373	103.2994324	3594.677919
92	31.40806849	37.08615677	103.2979454	3718.853285
93	31.88457944	36.14866044	103.3104174	3610.714708
94	44.46826442	48.03517628	103.2911984	5008.981101
95	43.66052997	46.41320715	99.89648801	4718.987877
96	43.65870309	48.03963579	103.2152316	4931.367639

Table A.4. Continued.

97	43.68276098	48.53963144	103.2338602	4919.800459
98	43.73807279	47.46101098	103.2430333	4762.040244

Table A.5.

Data for the second stage of compressor operation comprising of refrigerant temperatures.

Test	$T_{out,ref,evap}$	$T_{out,ref,comp}$	$T_{out,ref,cond}$	$T_{sat,evap}$
[-]	[°C]	[°C]	[°C]	[°C]
0	25.59289003	75.16641944	35.74882353	8.673299233
1	25.74129534	80.55398964	40.84373057	10.1473057
2	25.22985836	75.37611898	35.59563739	8.128441926
3	24.7485439	76.25059957	35.30788009	7.128436831
4	25.41971487	76.41360489	35.65678208	7.944154786
5	25.77640569	76.22462633	35.82822064	8.501067616
6	26.11352941	82.0702451	41.9347549	10.36272059
7	26.2367474	87.5499308	46.70764706	11.75581315
8	25.7115	82.2533	41.81698	9.99056
9	25.06924342	83.52458882	41.69638158	8.983256579
10	25.9044774	83.70858757	42.09882768	9.916468927
11	26.31363636	83.46564738	41.98752066	10.33982094
12	26.10449541	91.27545872	48.30940367	11.27715596
13	26.83688525	96.71599532	53.30826698	13.54266979
14	26.70848958	92.26755208	49.43838542	12.13694444
15	25.92730296	91.17598522	47.91805419	11.31393473
16	26.57651803	91.37794592	48.31671252	12.06064991
17	26.76693391	91.0766143	48.35589924	12.38358072
18	25.29657328	81.40681034	43.27090517	11.35810345
19	25.64968085	86.24723404	47.8493617	13.33010638
20	25.56991903	80.6248583	43.01259109	11.8692915
21	24.20268627	81.18427451	42.07309804	10.36376471
22	25.09091062	81.44411467	42.59131535	11.38177066
23	25.54102564	81.23376068	42.82731624	12.03591453
24	24.64698745	73.45577406	36.41623431	9.709958159
25	23.95179592	73.87918367	35.53267347	8.580673469
26	25.48206089	88.72	49.26461358	13.02599532
27	26.56837423	95.02880368	54.65636503	15.35846626
28	26.45482645	90.26333884	50.71252893	14.00061157
29	24.82283358	88.81832084	48.20053973	12.1673913

Table A.5. Continued.

30	25.74060948	89.30935666	48.91137698	13.21046275
31	26.39695397	89.33866946	49.34642678	14.04268619
32	22.68310782	71.60866808	35.45926004	9.178287526
33	25.23975078	78.71358255	42.17146417	12.29956386
34	25.20952632	72.52115789	36.41139474	11.02578947
35	23.87003565	71.84650624	35.97294118	10.56522282
36	24.50117359	72.87787286	36.2600978	10.09745721
37	24.67164557	71.48873418	36.09848101	11.54544304
38	24.95833333	80.78369478	43.31034137	11.67301205
39	25.52335632	85.58303448	47.86763218	13.60004598
40	25.52217565	79.90381238	43.0098004	12.37856287
41	22.75072106	79.46178368	42.37206831	11.05388994
42	24.03699145	79.43300855	42.61581197	12.07495726
43	24.68705983	79.29015385	42.87682051	12.86247863
44	23.96582178	87.5450297	49.9630099	13.34619802
45	24.80822785	94.03599156	55.02527426	15.09424051
46	24.74320843	87.23824356	49.92192037	13.91327869
47	23.33642265	87.59502762	49.03298343	12.9121547
48	24.67800185	87.85521739	49.47100833	13.96788159
49	25.34644956	87.80299444	49.71069102	14.57168388
50	24.51873684	84.89182456	48.16189474	13.60526316
51	24.40387302	78.1715873	42.56809524	12.4031746
52	22.99509213	77.88450586	42.87458961	12.5381072
53	21.66936782	76.55264368	42.17094828	11.82663793
54	24.02315299	78.00649254	43.08154851	13.40712687
55	21.62534247	69.63735812	35.92156556	10.382818
56	24.16840782	75.91122905	41.1273743	12.31589385
57	24.22834025	69.66454357	35.23607884	11.20755187
58	22.77272201	70.24866795	36.14789575	11.07596525
59	23.68502083	70.08295833	36.247375	12.10683333
60	25.27181189	88.69767635	50.94784232	14.23556017
61	23.74795203	86.68642066	49.40896679	13.72856089
62	24.7052	86.41666667	49.1752	14.38615
63	22.73434146	85.50256098	49.11568293	13.54478049
64	19.33155009	67.99860113	35.57172023	9.789867675
65	21.64307229	69.16128514	35.52218876	11.29267068
66	22.72301887	69.55122642	35.10588679	12.18307547
67	19.00977346	74.65838188	41.7479288	11.40349515
68	22.95902439	76.78356473	41.884803	13.85679174

Table A.5. Continued.

69	21.68528509	76.29364035	42.06320175	12.80166667
70	19.72265795	85.46496732	48.65405229	13.17204793
71	22.95792342	85.61562592	47.83213549	14.57602356
72	21.96715232	85.22346026	48.39218543	13.93887417
73	19.6772973	74.80276507	39.25413721	12.63401247
74	20.90319672	75.89300546	38.90887978	13.15617486
75	16.86307522	74.46013274	38.84334071	11.00966814
76	16.0313879	64.87683274	33.00619217	9.748042705
77	19.85440882	67.42182365	33.02747495	11.13106212
78	21.44776447	68.03656687	32.53996008	12.10127745
79	17.27916667	84.89405303	44.47649621	12.24835227
80	20.24883481	85.46668142	44.92348083	13.59842183
81	21.51418792	85.82374497	44.38805369	14.10238926
82	16.18277251	76.39509479	35.80338863	10.3935545
83	19.1048	74.75994286	35.67725714	11.80942857
84	19.05548708	76.07395626	36.44459245	12.0326839
85	19.91202417	86.8031571	41.14697885	13.7576435
86	19.99895238	73.75019048	35.79163492	12.87628571
87	20.1923662	77.43895775	37.88549296	13.40490141
88	19.67881466	78.24778017	36.02984914	12.81571121
89	15.65095023	66.41468326	29.36780543	9.23800905
90	18.73190299	68.59227612	31.2344403	11.29893657
91	18.87571429	67.265686	30.49205092	11.20304102
92	20.29616438	69.25365297	31.2053653	12.26207763
93	20.46641121	68.08231776	30.45020561	12.22988785
94	19.79647837	90.78112981	43.45040865	13.09280048
95	16.47028391	85.77050473	42.47927445	11.23899054
96	18.73135392	88.10171021	43.35349169	12.93083135
97	20.04494309	88.4023252	43.66744715	14.00352846
98	20.11610052	86.44951473	43.07466205	13.84386482

Table A.6.

Data for the second stage of compressor operation comprising of refrigerant pressures.

Test	$P_{in,ref,comp}$	$P_{out,ref,comp}$	$P_{out,ref,cond}$
[-]	[kPa]	[kPa]	[kPa]
0	961.7093197	2301.625481	2195.394171
1	996.3769948	2613.796896	2504.240611

Table A.6. Continued.

2	951.6407989	2293.214204	2190.444742
3	927.6153619	2283.445214	2182.250251
4	949.4155601	2301.636051	2198.786236
5	968.5004911	2314.920673	2209.904075
6	1001.043203	2661.935017	2554.621662
7	1037.410121	2989.66892	2878.653422
8	983.985762	2647.305494	2539.770294
9	971.1162796	2653.01049	2550.211551
10	990.4419153	2679.112825	2575.025114
11	1004.17343	2684.705004	2579.812876
12	1002.165298	3060.441229	2953.609046
13	1060.072108	3435.182752	3326.112691
14	1027.803655	3154.955925	3047.366953
15	1017.677398	3055.413956	2950.322465
16	1036.397339	3077.755344	2970.582448
17	1050.091878	3091.200556	2985.453087
18	1038.237302	2767.195047	2662.260265
19	1086.342777	3088.445822	2981.441059
20	1055.244947	2752.721834	2646.841296
21	1007.586102	2709.912022	2600.589788
22	1035.115	2738.441976	2628.371853
23	1055.502402	2752.865338	2642.627014
24	995.9169623	2357.664142	2253.013322
25	968.0286837	2315.835143	2210.125639
26	1069.193763	3152.453946	3044.18718
27	1136.359983	3571.96204	3463.739486
28	1103.730469	3272.635873	3163.43045
29	1062.748777	3136.325244	3023.311948
30	1086.990431	3172.545558	3058.499315
31	1105.520308	3186.830577	3074.121581
32	984.4118964	2320.64471	2212.404854
33	1068.513994	2725.327131	2617.552162
34	1038.897232	2366.802234	2260.002724
35	1029.28654	2357.640542	2244.861148
36	1012.036944	2351.87991	2248.486716
37	1056.671848	2377.451025	2260.577013
38	1050.093554	2774.506275	2671.266295
39	1101.017106	3094.793754	2988.555678
40	1069.95423	2753.248507	2648.268154
41	1022.038011	2721.544989	2611.327245

Table A.6. Continued.

42	1058.216674	2746.588944	2633.439244
43	1086.444279	2769.546851	2657.230072
44	1088.208491	3225.866244	3120.459529
45	1137.419348	3607.987996	3507.518778
46	1106.828733	3217.62437	3113.41281
47	1067.633318	3165.87407	3055.852815
48	1108.97837	3200.954543	3088.536798
49	1127.768565	3221.493871	3109.946543
50	1106.647863	3123.364649	3019.645091
51	1079.339698	2740.125495	2633.758724
52	1078.876218	2776.851678	2664.032677
53	1055.710678	2721.141736	2614.427549
54	1110.764815	2800.843306	2687.613511
55	1021.220256	2350.101045	2239.399352
56	1078.099017	2672.869492	2561.854763
57	1054.219525	2325.722315	2212.052971
58	1049.408541	2382.711467	2264.851948
59	1081.376254	2406.645573	2284.364421
60	1131.2794	3311.944154	3210.420975
61	1115.296456	3214.057292	3109.621011
62	1148.36294	3238.779662	3131.668853
63	1097.785334	3173.118651	3072.994695
64	1009.370879	2372.845624	2259.19924
65	1056.126207	2414.560574	2296.700323
66	1086.389626	2444.496504	2324.372632
67	1042.466411	2728.792375	2621.420019
68	1121.085287	2822.212015	2709.540319
69	1091.66732	2795.306496	2685.623031
70	1079.590682	3284.296673	3184.814797
71	1137.831449	3273.529853	3169.74399
72	1117.493515	3250.730257	3146.765738
73	1098.005318	2851.144728	2743.176541
74	1119.278811	2879.290954	2773.741913
75	1039.324332	2817.690376	2724.659867
76	1007.666868	2377.233847	2274.525377
77	1061.268916	2425.35199	2312.118768
78	1095.897373	2457.230627	2341.445447
79	1062.656091	3333.488386	3251.337801
80	1115.433816	3340.616864	3245.93282

Table A.6. Continued.

81	1139.836987	3365.510239	3272.506515
82	1029.921531	2922.787339	2841.262495
83	1082.326526	2846.948423	2760.132909
84	1085.776085	2929.926674	2841.3247
85	1134.372739	3527.09174	3445.079446
86	1115.460251	2844.513341	2750.376387
87	1126.859718	3036.683899	2944.380532
88	1120.367978	3085.192291	2993.102375
89	1002.678984	2454.010738	2363.815034
90	1071.529349	2572.555715	2474.865642
91	1068.302479	2509.025344	2410.703963
92	1107.352817	2610.961614	2510.312489
93	1104.288542	2543.726045	2442.650398
94	1104.359276	3577.021998	3497.752438
95	1044.078874	3392.741546	3319.739644
96	1097.457095	3531.330675	3451.157081
97	1142.463496	3576.00955	3494.599125
98	1141.186799	3473.612392	3393.421024

Appendix B. Experimental Data From Open Lab Testing

Table B.1.

Data from open lab testing comprising of refrigerant temperatures and pressures.

Test	Compressor stage	$T_{out,ref,evap}$	$T_{out,ref,comp}$	$T_{out,ref,cond}$	$T_{sat,evap}$	$P_{in,ref,comp}$	$P_{out,ref,cond}$
[-]	[-]	[°C]	[°C]	[°C]	[°C]	[kPa]	[kPa]
0	1	19.28	62.41	26.71	3.77	862.97	1753.04
1	1	20.47	60.68	26.91	5.43	906.4	1764.08
2	1	21.12	66.08	33.45	8.81	989.56	2082.07
3	1	21.07	61.18	29.35	7.77	966.05	1869.59
4	1	21.26	59.89	27.4	6.61	940.65	1789.87
5	1	18.73	60.34	27.31	5.41	901.83	1772.1
6	1	20.37	58.96	27.73	7.51	967.37	1804.78
7	1	20.9	58	27.92	8.41	999.08	1818.61
8	1	20.9	59.87	29.86	8.98	1008.59	1907.76
9	1	20.79	65.35	34.15	9.74	1022.94	2133.09
10	1	17.5	58.93	27.58	5.72	915.95	1794.86
11	1	19.55	57.72	27.92	7.9	987.18	1822.78
12	1	19.18	65.5	33.88	8.51	987.41	2124.06
13	1	19.24	59.56	29.28	7.8	977.83	1885.11
14	1	20.46	56.64	28.1	9.1	1014.83	1836.5
15	1	15.16	57.07	26.97	4.87	893.91	1774.47
16	1	18.46	57.23	28.29	7.83	980.75	1845.11
17	1	18.97	65.43	35.13	9.51	1018.67	2205.23
18	1	19.21	59.45	30.46	8.79	1006.17	1947.94
19	1	19.68	56.67	28.51	8.98	1018.32	1861.16
20	1	14.76	56.49	28.02	6.11	930.04	1834.29
21	1	18.47	55.71	28.49	8.97	1018.52	1870.89
22	1	19.58	65.23	36.72	11.44	1092.82	2321.51
23	1	19.83	58.41	31.41	10.73	1072.35	2018.96
24	1	19.37	54.8	28.48	9.99	1050.01	1876
25	1	11.87	54.98	27.53	5.13	914.48	1840.57
26	1	15.61	54.19	27.62	7.85	996.52	1856.88
27	1	16.97	63.94	33.44	9.96	1061.4	2298.62
28	1	17.28	56.48	29.48	9.59	1044.72	1987.86
29	1	17.71	53.57	26.91	9.48	1044.33	1865.06
30	1	15.2	55.29	25.79	8.08	1004.09	1924.96
31	1	16.68	67.26	30.92	9.96	1058.49	2440.38
32	1	17.04	58.34	27.22	9.63	1050.23	2076.86

Table B.1. Continued.

33	1	17.38	54.83	26.14	9.79	1053.4	1943.16
34	1	11.6	55.74	25.69	5.14	917.73	1890.58
35	2	20.09	67.59	27.9	2.83	809.94	1818.18
36	2	20.54	66.86	28.16	3.64	835.96	1833.67
37	2	21.26	68.68	31.32	5.94	885.95	1975.07
38	2	21.17	66.7	29.38	5.47	874.86	1877.81
39	2	20.85	66.51	28.46	4.24	853.38	1849.61
40	2	20.15	65.67	28.76	5.32	877.6	1861.64
41	2	20.6	64.94	28.95	6.19	900.86	1873.93
42	2	20.85	64.47	29.17	6.78	918.71	1885.67
43	2	20.73	66.76	31.5	7.21	919.13	1990.75
44	2	20.84	64.81	29.59	6.96	917.59	1900.93
45	2	18.92	64	28.91	5.85	893.77	1878.18
46	2	19.64	63.39	29.1	6.93	923.36	1892.39
47	2	19.86	66.23	32	7.67	932.06	2023.34
48	2	19.44	64.18	29.42	6.48	905.47	1899.84
49	2	20.15	63.04	29.34	7.69	955.24	1910.93
50	2	17.67	62.32	28.71	6.2	902.72	1880.02
51	2	18.59	61.68	28.83	7.38	936.04	1892.51
52	2	18.75	64.2	31.66	8.17	955.72	2032.87
53	2	19.11	62.34	29.62	8.05	956.76	1940.55
54	2	19.17	61.07	28.85	8.41	970.77	1908.86
55	2	15.44	59.88	28.43	6.35	910.3	1896.21
56	2	16.99	59.81	28.2	7.55	944.69	1899.5
57	2	17.96	63.06	31.15	9.05	988.99	2077.47
58	2	18.72	61.22	28.85	9.13	996.73	1978.47
59	2	18.11	60.27	27.6	8.22	967.51	1925.65
60	2	13.9	58.78	26.04	6.62	932.12	1946.04
61	2	15.81	58.71	25.83	7.9	969.81	1949.33
62	2	18.46	62.76	27.91	10.46	1048.46	2174.42
63	2	18.48	60.31	25.89	10.05	1035.68	2037
64	2	16.85	59.72	25.06	8.16	980.61	1964.07
65	2	12.79	59.48	23.5	6.05	923.67	2012.39
66	2	14.55	59.47	23.69	7.37	961.03	2024.87
67	2	15.49	63.35	25.37	8.29	985.72	2217.93
68	2	15.75	60.47	24.16	8.21	986.63	2079.74
69	2	16.13	59.8	23.78	8.4	991.39	2041.3

Appendix C. Open Lab Testing Matrix

Table C.1.

Open lab testing matrix for the first stage of operation

Charge level [-]	Condenser PWM duty cycle [%]	Evaporator PWM duty cycle [%]
0.6	70	20
0.6	70	40
0.6	30	60
0.7	70	20
0.7	70	40
0.7	70	60
0.7	50	60
0.7	30	60
0.8	70	20
0.8	70	40
0.8	70	60
0.8	50	60
0.8	30	60
0.9	70	20
0.9	70	40
0.9	70	60
0.9	50	60
0.9	30	60
1	70	20
1	70	40
1	70	60
1	50	60
1	30	60
1.1	70	20
1.1	70	40
1.1	70	60
1.1	50	60
1.1	30	60
1.2	70	20
1.2	70	40
1.2	70	60
1.2	50	60
1.2	30	60

Table C.2.

Open lab testing matrix for the second stage of operation

Charge level [-]	Condenser PWM duty cycle [%]	Evaporator PWM duty cycle [%]
0.6	100	50
0.6	100	70
0.6	100	90
0.7	100	50
0.7	100	70
0.7	100	90
0.7	80	90
0.7	60	60
0.8	100	50
0.8	100	70
0.8	100	90
0.8	80	90
0.8	60	60
0.9	100	50
0.9	100	70
0.9	100	90
0.9	80	90
0.9	60	60
1	100	50
1	100	70
1	100	90
1	80	90
1	60	60
1.1	100	50
1.1	100	70
1.1	100	90
1.1	80	90
1.1	60	60
1.2	100	50
1.2	100	70
1.2	100	90
1.2	80	90
1.2	60	60

Appendix D. Python Program Code

C.1. Virtual Refrigerant Charge Sensor

```
# -*- coding: utf-8 -*-
Created on Wed Jan 29 18:47:32 2014

@author: Jebaraj
"""
#Importing the necessary libraries for code
import os
import pylab
import numpy as np
import statsmodels.api as sm
from sklearn.metrics import mean_squared_error
import matplotlib.pyplot as plt
from matplotlib.ticker import MaxNLocator
from pandas import *

#Clearing system memory
os.system('cls')

#Importing necessary data files for analysis
types= read_excel(r'C:\Users\Jebaraj_PC\SkyDrive\Research\Diagnostics
thesis\Diagnostics thesis\Lennox Microchannel\Data\Open lab
training\training_data.xlsx',
'Firststage_VRC_training')
data = DataFrame(types)

#Formulating x1 to contain the necessary independent variables in the model
x1 = data[['Del_T_sub','Del_T_sh','Del_Q']]

#Formulating y1 to contain the dependent variable
y1= data['m_ratio_act']
y1=y1-1.0
#weights= data['norm weights']

#Learning the coefficients of the model using OLS routine
model = sm.OLS(y1,x1)
#model_wls = sm.WLS(y1,X,weights)
#fit_WLS= model_wls.fit()
#print fit_WLS.summary()
#param=fit_WLS.params
fit = model.fit()
print fit.summary()
```

```
param = fit.params
#Using the learned coefficients to predict the dependent variable
y=
np.ones(len(y1)).T+param[0]*x1['Del_T_sub']+param[1]*x1['Del_T_sh']+param[2]*x1['
Del_Q']
y1=y1+1.
y=y*100.
y1=y1*100

#Calculating the root mean square error of the model
rms = np.sqrt(mean_squared_error(y1,y))
x= data['m_ratio_act']
print rms
f=plt.figure()
mad = max(np.abs(y - y1))
print mad

#plotting the predicted and measured values of the dependent variable by means of a
scatter plot

ax= f.add_subplot(111)
p=ax.scatter(y1, y, marker='o',color='b')
x_lims = [50,140]
y_lims = [50,140]
lims = (min(x_lims[0], y_lims[0]), max(x_lims[1], y_lims[1]))
# lims = (min(np.min((x, y), axis=1)), max(np.max((x, y), axis=1))
ax.plot(lims,lims,'k-')
#x_lims = plt.xlim()
#y_lims = plt.ylim()

plt.axis('scaled')
a=10
ax.set_xlim(x_lims)
ax.set_ylim(y_lims)
ax.plot(np.array(lims), np.array(lims) + a,'k--')
ax.plot(np.array(lims), np.array(lims) - a,'k--')
ax.set_xlabel('Measured Refrigerant charge[%]',fontsize=15,fontweight="bold")
ax.set_ylabel('Predicted Refigerant charge[%]',fontsize=15,fontweight="bold")
ax.tick_params(axis='both', which='major', labelsize=13)
ax.legend()
ax.grid(True)
plt.show()
plt.text(0.65,0.9,r"Maximum deviation=$\pm$%0.1f"%(mad)+"%" , ha='right',
va='bottom', transform=ax.transAxes, fontsize=14)
```

```
ax.text(0.95,0.1,r"RMSE=$\pm$%0.1f"%(rms)+"%" , ha='right', va='bottom',
transform=ax.transAxes, fontsize=14)
#ax.legend([p1,p2],['First stage', 'Second stage'],loc='upper left', ncol=1)
ax.text(0.4,0.55,'+10%', ha='center', va='center', transform=ax.transAxes,
fontsize=14,rotation=45)
ax.text(0.55,0.4,'-10%', ha='center', va='center', transform=ax.transAxes,
fontsize=14,rotation=45)
plt.savefig(r'C:\Users\Jebaraj_PC\SkyDrive\Research\Latex Files\Thesis final\Thesis
outline\Thesis plots\VRC sensor\VRC_model3_1stage.png', bbox_inches='tight')
```

C.2. Algorithm for Selecting Optimal Open lab testing Data

```
# -*- coding: utf-8 -*-
"""
Created on Sat Jul 25 20:17:14 2015

@author: Jebaraj_PC
"""
#importing necessary libraries for the code
import numpy as np
import pdb
import pandas as pd
import statsmodels.api as sm
import os
import matplotlib.pyplot as plt
from sklearn.metrics import mean_squared_error
import matplotlib as mpl
from mpl_toolkits.mplot3d import Axes3D
os.system('cls')
plt.close('all')


def data_train(filepath=r'C:\Users\Jebaraj_PC\SkyDrive\Research\Diagnostics
thesis\Diagnostics thesis\Lennox Microchannel\Data\Open lab
training\training_data.xlsx', sheetname='Secondstage_VRC_training'):

# Read the train data from excel spreadsheet into a data frame.
        data = pd.read_excel(filepath, sheetname)

        return data

def data_test(filepath=r'C:\Users\Jebaraj_PC\SkyDrive\Research\Diagnostics
thesis\Diagnostics thesis\Lennox Microchannel\Data\Psychroom\Test
data\Overall_Summary-Jebaraj.xlsx', sheetname='Secondstage_VRC_testing'):
```

```
# Read the test data from excel spreadsheet into a data frame.
        data = pd.read_excel(filepath, sheetname)

        return data


def plotting(x1,X):

#Function to plot the independent variables against each other in a 2d-scatter plot
        data = data_train()
        f= plt.figure(**dict(figsize=(8, 6)))
        ax= f.add_subplot(111)
        cb_ax, cb_kw = mpl.colorbar.make_axes([ax], pad=0.05)
        X=np.array(X)
        cmap=plt.cm.jet
        z = data['m_ratio_act']
        #tick_locator = mpl.ticker.MaxNLocator(nbins=4)
        #color = colors.next()
        p = ax.scatter(x1['Del_T_sh'], x1['Del_T_sub'],c=z,s=200)
        ax.grid(True)
        ax.scatter(X[:,2], X[:,1],color='black',s=70,marker='D')
        v=[0.6,0.7,0.8,0.9,1.0,1.1,1.2]
        cb = f.colorbar(p,cax=cb_ax, ticks=v,cmap=cmap, **cb_kw)
        cb.ax.tick_params(labelsize=15)
        cb.solids.set_edgecolor('face')
        cb.set_label('Charge level [-]', fontsize=15,fontweight="bold",
        rotation=270,labelpad=15)
        ax.set_xlabel('T_sh-T_sh$\mathbf{_{rated}}$
        [$^{\circ}$C]',fontsize=15,fontweight="bold")
        ax.set_ylabel('T_sub-T_sub$\mathbf{_{rated}}$[$^{\circ}$C]',
        fontsize=15,fontweight="bold")
        ax.set_title('5-point optimal design',fontsize=15,fontweight="bold")
        ax.tick_params(axis='both', which='major', labelsize=15)
        plt.savefig(r'C:\Users\Jebaraj_PC\SkyDrive\Research\Diagnostics
        thesis\Diagnostics thesis\Lennox Microchannel\Data\Psychroom\Test
        data\Images\Optimality\plot2d_sub_sh.png', bbox_inches='tight')
        return

def plotting3D(x1,X):

#Function to plot the independent variables against each other in a 3d-scatter plot

        data = data_train()
        f= plt.figure(**dict(figsize=(8, 6)))
        ax= f.add_subplot(111,projection='3d')
```

```
        cb_ax, cb_kw = mpl.colorbar.make_axes([ax], pad=0.05)
        X=np.array(X)
        cmap=plt.cm.jet
        z = data['m_ratio_act']
        #tick_locator = mpl.ticker.MaxNLocator(nbins=4)
        #color = colors.next()
        p = ax.scatter(x1['Del_T_sub'], x1['Del_T_sh'],x1['Del_Q'],c=z,s=200)
        p.set_edgecolors = p.set_facecolors = lambda *args:None
        ax.grid(True)
        ax.scatter(X[:,1], X[:,2], X[:,3],color='black',s=70,marker='D')
        v=[0.6,0.7,0.8,0.9,1.0,1.1,1.2]
        cb = f.colorbar(p,cax=cb_ax, ticks=v,cmap=cmap, **cb_kw)
        cb.ax.tick_params(labelsize=15)
        cb.solids.set_edgecolor('face')
        cb.set_label('Charge level [-]', fontsize=15,fontweight="bold",
        rotation=270,labelpad=15)
        ax.set_xlabel('T_sub-T_sub$\mathbf{_{rated}}$
        [$^{\circ}$C]',fontsize=15,fontweight="bold")
        ax.set_ylabel('T_sh-T_sh$\mathbf{_{rated}}$[$^{\circ}$C]',
        fontsize=15,fontweight="bold")
        ax.set_zlabel('x_evap-x_evap$\mathbf{_{rated}}$[-]',
        fontsize=15,fontweight="bold")
        ax.set_title('optimal design',fontsize=15,fontweight="bold")
        ax.xaxis._axinfo['label']['space_factor'] = 2.1
        ax.yaxis._axinfo['label']['space_factor'] = 2.1
        ax.zaxis._axinfo['label']['space_factor'] = 2.1
        ax.tick_params(axis='both', which='major', labelsize=15)
        plt.savefig(r'C:\Users\Jebaraj_PC\SkyDrive\Research\Diagnostics
        thesis\Diagnostics thesis\Lennox Microchannel\Data\Psychroom\Test
        data\Images\Optimality\plot3d_optimalpoints_firststage.png',
        bbox_inches='tight')
        return


def train(X):

#Function takes in the optimal experimental points from optimal function and learns the
coefficient of the VRC model

        data = data_train()
        z = data['m_ratio_act']
        #indices= np.where(np.in1d(x1['Del_T_sub'],X[:,1])==True)
        y=[]
        indices=[]
        x1 = data[['Del_T_sub','Del_T_sh','Del_Q']]
```

```
x1=np.matrix(x1)
for i in range(len(X[:,0:4])):
        for j in range(len(x1)):
                if np.array_equal(X[:,0:4][i],x1[j]):
                        y.append(z[j])
                        indices.append(j)
y=np.array(y)
print y
y=y-1.0

#Learn the model coefficients using OLS routine
model = sm.OLS(y,X)
fit = model.fit()
print fit.summary()
param = fit.params

#Formulating x1 to include the independent variables in the model
x1 = data[['Del_T_sub','Del_T_sh','Del_Q']]
y1= param[0]*X[:,0]+param[1]*X[:,1]+param[2]*X[:,2]
# print y1
#pdb.set_trace()
q=np.empty(np.shape(y1))
e=np.empty(np.shape(y1))
for i in range(len(indices)):
q[i]= data.ix[indices]['Cond_PWM'].values[i]
e[i]=data.ix[indices]['Evap_PWM'].values[i]
print q
print e
data = data_test()
z = data['m_ratio_act']
Pred_Charge=np.ones(len(z)).T+param[0]*data['Del_T_sub']+param[1]*data['Del
_T_sh']+param[2]*data['Del_Q']

#Plotting the scatter plot for the predicted and measured values of the dependent
variable
f= plt.figure(**dict(figsize=(8, 6)))
ax= f.add_subplot(111)
plt.plot(z, Pred_Charge, 'o',markersize=5)
x_lims = [0.5,1.3]
y_lims = [0.5,1.3]
lims = (min(x_lims[0], y_lims[0]), max(x_lims[1], y_lims[1]))
plt.plot(lims,lims,'k-')
plt.axis('scaled')
a=0.1
plt.xlim(lims)
```

```
        plt.ylim(lims)
        plt.plot(np.array(lims), np.array(lims) + a,'k--')
        plt.plot(np.array(lims), np.array(lims) - a,'k--')
        plt.xlabel('Actual Refrigerant charge[-]',fontsize=15,fontweight="bold")
        plt.ylabel('Virtual Refigerant charge[-]',fontsize=15,fontweight="bold")
        rms = np.sqrt(mean_squared_error(z,Pred_Charge))
        print rms
        plt.text(0.95,0.1,r"RMSE=$\pm$%0.2f"%(rms) , ha='right', va='bottom',
        transform=ax.transAxes, fontsize=14)
        plt.tick_params(axis='both', which='major', labelsize=13)
        plt.legend()
        plt.grid(True)
        plt.show()

def optimal(p):

#Function takes in the number of points and returns the optimal experimental runs
corresponding to the input number of data points

        data = data_train()
        x1 = data[['Del_T_sub','Del_T_sh','Del_Q']]
        Epsilon=x1
        Epsilon=np.matrix(Epsilon)
        rand= np.random.permutation(len(Epsilon))
        n= len(Epsilon)-p
        X= Epsilon[rand[0:p],:]
        Epsilon2=np.matrix(np.empty((n,p)))
        Epsilon2=Epsilon[rand[p:],:]
        d=np.empty((n,p))
        while True:
                #pdb.set_trace()
                #print np.linalg.det(X.T*X)/p
                for i in range(n):
                d_j= Epsilon2[i]*(X.T*X).I*Epsilon2[i].T
                        for j in range(p):
                                d_i= X[j,:]*(X.T*X).I*X[j,:].T
                                d_i_j= X[j,:]*(X.T*X).I*Epsilon2[i].T
                                d[i,j]= d_j- (d_i*d_j- d_i_j*d_i_j)-d_i
                #print d
                if np.max(d)>0:
                        ix,ij= np.where(d==np.max(d))
                        a=Epsilon2[ix]
                        Epsilon2[ix]=X[ij,:]
                        X[ij,:]=a
                else:
```

```
                    break
        train(X)


if __name__ == '__main__':
        data = data_train()
        x1 = data[['Del_T_sub','Del_T_sh','Del_Q']]
        Epsilon=x1
        #Epsilon = sm.add_constant(x1)
        Epsilon=np.matrix(Epsilon)
        det= []
        trace=[]
        rand= np.random.permutation(len(Epsilon))
        for p in range(3,len(x1)):
                n= len(Epsilon)-p
                X= Epsilon[rand[0:p],:]
                Epsilon2=np.matrix(np.empty((n,p)))
                Epsilon2=Epsilon[rand[p:],:]
                d=np.empty((n,p))
                while True:
                        #pdb.set_trace()
                        #print np.linalg.det(X.T*X)/p
                        for i in range(n):
                                d_j= Epsilon2[i]*(X.T*X).I*Epsilon2[i].T
                                for j in range(p):
                                        d_i= X[j,:]*(X.T*X).I*X[j,:].T
                                        d_i_j= X[j,:]*(X.T*X).I*Epsilon2[i].T
                                        d[i,j]= d_j- (d_i*d_j- d_i_j*d_i_j)-d_i
                        #print d
                        if np.max(d)>0:
                                ix,ij= np.where(d==np.max(d))
                                a=Epsilon2[ix]
                                Epsilon2[ix]=X[ij,:]
                                X[ij,:]=a
                        else:
                                det.append((np.linalg.slogdet(X.T*X)[1]))
                                trace.append(np.log(np.trace((X.T*X).I)))
                                #print det
                                break
det=np.array(det)

#Threshold of 90% of the maximum determinant of the information matrix
opt= len(det[det<=0.9*np.max(det)])+3
print opt
```

```
#Plotting the change in determinant and trace of the information matrix
f=plt.figure()
ax= f.add_subplot(211)
plt.plot(range(3,len(x1)),det)
xlim=[3,34]
ax.set_xlim(xlim)
#plt.plot((17, 17), (0, 0), 'k-')
ax.axvline(x=opt,c="black",linewidth=2.0,zorder=0)
ax.axhline(y=0.9*np.max(det),c="black",linewidth=2.0,zorder=0)
plt.legend()
plt.grid(True)
ax.text(0.85,0.8,r"90% of max(det(X$^{T}$X))", ha='right', va='bottom',
transform=ax.transAxes, fontsize=12)
plt.ylabel('det(X$^{T}$X)',fontsize=15,fontweight="bold")
plt.tick_params(axis='both', which='major', labelsize=13)
ax=f.add_subplot(212,sharex=ax)
ax.set_xlim(xlim)
plt.plot(range(3,len(x1)),trace)
ax.axvline(x=opt,c="black",linewidth=2.0,zorder=0)
plt.ylabel('trace((X$^{T}$X)$^{-1}$)',fontsize=15,fontweight="bold")
plt.legend()
plt.grid(True)
plt.xlabel('No. of optimal experimental runs',fontsize=15,fontweight="bold")
f.tight_layout()
plt.show()
plt.savefig(r'C:\Users\Jebaraj_PC\SkyDrive\Research\Diagnostics thesis\Diagnostics
thesis\Lennox Microchannel\Data\Psychroom\Test
data\Images\Optimality\DetVsnoofruns_first stage', bbox_inches='tight')
print opt

#Calling the respective functions
optimal(opt)
plotting3D(x1,X)
plotting(x1,X)
train(X)
```